การจำลองแบบสมูทพาร์ทิเคิลไฮโดรไดนามิกส์สำหรับการเคลื่อนที่

ของหยดน้ำบนผิวแนวดิ่ง

นายชัยยศ กำธรเจริญ

วิทยานิพนธ์นี้เป็นส่วนหนึ่งของการศึกษาตามหลักสูตรปริญญาวิทยาศาสตรมหาบัณฑิต

สาขาวิชาคณิตศาสตร์ประยุกต์และวิทยาการคณนา

ภาควิชาคณิตศาสตร์และวิทยาการคอมพิวเตอร์

คณะวิทยาศาสตร์ จุฬาลงกรณ์มหาวิทยาลัย

ปีการศึกษา 2557

ลิขสิทธิ์ของจุฬาลงกรณ์มหาวิทยาลัย

SMOOTHED PARTICLE HYDRODYNAMICS SIMULATION
FOR WATER DROPLET MOTION ON VERTICAL SURFACE

Mr. Chaiyod Kamthorncharoen

A Thesis Submitted in Partial Fulfillment of the Requirements
for the Degree of Master of Science Program in Applied Mathematics and
Computational Science
Department of Mathematics and Computer Science
Faculty of Science
Chulalongkorn University
Academic Year 2014

Thesis Title   SMOOTHED PARTICLE HYDRODYNAMICS SIMULATION FOR WATER DROPLET MOTION ON VERTICAL SURFACE

By   Mr. Chaiyod Kamthorncharoen

Field of Study   Applied Mathematics and Computational Science

Thesis Advisor   Kitiporn Plaimas, Dr.rer.nat

Accepted by the Faculty of Science, Chulalongkorn University in Partial Fulfillment of the Requirements for the Master's Degree

Deputy Dean, Acting Dean,

. . . . The Faculty of Science

(Associate Professor Somkiat Ngamprasertsith, Dr.de l'INPT)

THESIS COMMITTEE

. . . . Chairman

(Assistant Professor Khamron Mekchay, Ph.D.)

. . . . Thesis Advisor

(Kitiporn Plaimas, Dr.rer.nat.)

. . . . Examiner

(Ratinan Boonklurb, Ph.D.)

. . . . External Examiner

(Associate Professor Montri Maleewong, Ph.D.)

ชัยยศ กำธรเจริญ : การจำลองแบบสมูทพาร์ทิเคิลไฮโดรไดนามิกส์สำหรับการเคลื่อนที่ของหยดน้ำ
บนผิวแนวดิ่ง.
(SMOOTHED PARTICLE HYDRODYNAMICS SIMULATION FOR WATER DROPLET
MOTION ON VERTICAL SURFACE)
อ.ที่ปรึกษาวิทยานิพนธ์หลัก: ดร. กิติพร พลายมาศ, 52 หน้า.

การเคลื่อนที่ของหยดน้ำใน 2 และ 3 มิติบนพื้นผิวแนวจำลองโดยใช้วิธีสมูทพาร์ทิเคิลไฮโดรไดนา
มิกส์ซึ่งเป็นระเบียบวิธีที่ไม่ขึ้นอยู่กับกริด โดยในระเบียบวิธีนี้ของไหลจะถูกแบ่งออกเป็นชิ้นประกอบไม่
ต่อเนื่องเรียกแทนว่า "อนุภาค" การจำลองหยดน้ำที่เกาะติดกำแพงในแนวดิ่งอาศัยการแก้สมการนา-
เวียร์-สโตกส์ผสมกับแรงตึงผิว ซึ่งเกิดขึ้นจากปฏิสัมพันธ์ระหว่างอนุภาคโดยที่แตกต่างกันในบริบทของ
อนุภาคของไหลกับของไหล, อนุภาคของไหลกับของแข็งเปียก หรืออนุภาคของไหลกับของแข็งที่ไม่
เปียก ผลลัพธ์เชิงตัวเลขแสดงถึงผลของแรงตึงผิวที่ทำให้หยดน้ำเกาะติดกับกำแพง และการเปรียบ
เทียบสถานะของหยดน้ำว่าหยุดนิ่งหรือเคลื่อนที่ และการเปรียบเทียบมุมของหยดน้ำที่ได้จากการ
จำลองกับการทดลองจริงให้ผลที่สอดคล้องกัน

ภาควิชา	คณิตศาสตร์และ	ลายมือชื่อนิสิต ....
	วิทยาการคอมพิวเตอร์	ลายมือชื่อ อ.ที่ปรึกษาหลัก ....
สาขาวิชา	คณิตศาสตร์ประยุกต์และ	
	วิทยาการคณนา	
ปีการศึกษา	2557	

5572197723 : MAJOR APPLIED MATHEMATICS AND COMPUTATIONAL SCIENCE

KEYWORDS : DROPLET MOTION / SMOOTHED PARTICLE HYDRODY-NAMICS / SURFACE TENSION

CHAIYOD KAMTHORNCHAROEN : SMOOTHED PARTICLE HYDRO-DYNAMICS SIMULATION FOR WATER DROPLET MOTION ON VERTICAL SURFACE. ADVISOR : KITIPORN PLAIMAS, Dr.rer.nat, 52pp.

Two- and three-dimensional droplet movements are simulated on vertical direction by using smoothed particle hydrodynamics (SPH), which is a numerical meshfree method. With this technique, the fluid is divided into discrete elements, referred as "particles". Simulating the droplet hanging on the vertical wall, Navier-Stokes equation combined with the surface tension force which models from interaction between particles which is different in the context of fluid-fluid, fluid-wetted area, or fluid-not wetted area, is applied. The numerical results show the effect of surface tension that allows the droplets hanging on the wall and the comparison of droplet status, that is either retent or moving, and angles with the experimental data gives a good agreement.

Department	: Mathematics and Computer Science	Student's Signature ....
Field of Study	: Applied Mathematics and Computational Science	Advisor's Signature ....
Academic Year	: 2014	

ACKNOWLEDGEMENTS

First of all, I am deeply indebted to my supervisor, Dr. Kitiporn Plaimas for her helpful suggestions and encouragement throughout the course of this research. This thesis would not have been completed without all the support from her. In addition, I am deeply grateful to Professor Seiro Omata, Professor Karel Švadlenka, and Professor Norbert Pozar for giving me a precious studying experience when I was in Kanazawa, Japan.

I also would like to express my sincere thanks to the thesis committees, Assistant Professor Dr. Khamron Mekchay, Dr. Ratinan Boonklurb, Associate Professor Dr. Montri Maleewong for their valuable advices and comments.

Furthermore, I am very thankful to my dear friends and colleagues, especially Indonesian boy, namely Mr. Reza Rendian Septiawan who helped me not only in the study but also in typical life.

I would like to express my gratitude to the Development and Promotion of Science and Technology Talents Project (DPST) for the scholarship which I received throughout my undergraduate and graduate study.

At last, I heartily express my greatest thanks to my family who always be beside and support me with their best wishes.

CONTENTS

Page

LIST OF TABLES

Page

LIST OF FIGURES

Page

Page

Page

CHAPTER I

INTRODUCTION

1.1   Introduction to Droplet Motion

As we know that all things on the Earth suffer from the Earth's gravitational force which gives the same amount of the acceleration on them. Similarly, the droplet on the vertical plane suffers as well. However, the small droplet is sometimes stuck on the window glass. This is because there exists the fluid-solid attractive interaction (called adhesion) between the droplet and the vertical wall that holds the droplet from sliding down through the wall. For the small droplet, the adhesive interaction force beats the gravitational force, making the droplet is hanged on the wall. Whereas the mass of the droplet increases, the gravitational force acting on the droplet also increases, and finally the gravitational force beats the adhesion and the droplet falls under the gravitational force.

If we look closely into the droplet, we can find out that the droplet is similar to a spherical shape. This phenomenon is caused by fluid-fluid attractive interaction (which is called cohesion) which is relatively small compared to other interaction such as gravitational force or pressure force in and usually neglected in a macro-scaled case. However the droplet motion problem is grouped into micro-scaled problem, we must also consider the existence of the cohesion in our problem.

Both cohesion and adhesion properties of the fluid are caused by the surface tension force of the fluid. In most cases, surface tension force is neglected as it is relatively small compared to other governing forces on the fluid. But in the droplet motion problem, surface tension force must be considered and implemented into the problem. Later, we will explain about the equations govern the fluid motion in Chapter 2.

1.2 Objective of This Work

Droplet motion problem is an interesting case to be considered as it occurs commonly in our daily life, for example, a condensation drop occurs in the heat exchanger on many appliances such as air-conditioner and refrigerator [20]. In this work, we consider the droplet adhere to a wall under the gravitational force and surface tension. To keep the shape of droplet, the surface tension plays an important role. The droplet motion is governed by the Navier-Stokes equation which surface tension is added, alongside the mass conservation. Our goal is to simulate the droplet motion on vertical plane in 2- and 3-dimensional systems via Smoothed Particle Hydrodynamics (SPH) method combined with surface tension model and find the appropriate parameters providing the results as close as the realistic.
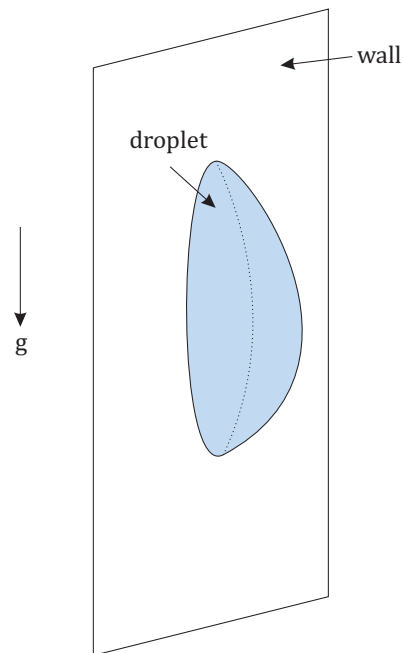
Figure 1.1: The droplet profile of our problem

1.3 Proposed Method

Smoothed Particle Hydrodynamics (SPH), a numerical meshfree method is applied here to solve the governing equations. Nowadays, it is one of the most

popular techniques used in simulating various types of the fluid flow problems. Its strategy is discretizing the fluid into a set of particles, which each particle carries its physical quantities, e.g. density, pressure, position, and velocity. The SPH approximation scheme is applied on governing equations. The particle total forces are calculated. Then, the particle velocity commonly comes out as a solution of Navier-Stokes equation via using the leapfrog integration scheme, and it is also used to update the particle position from the information of obtained particle velocity. Later, the explanation of the SPH and leapfrog integration scheme that used to solve this problem can be found in the Chapter 3. The below block diagram shows our proposed method.
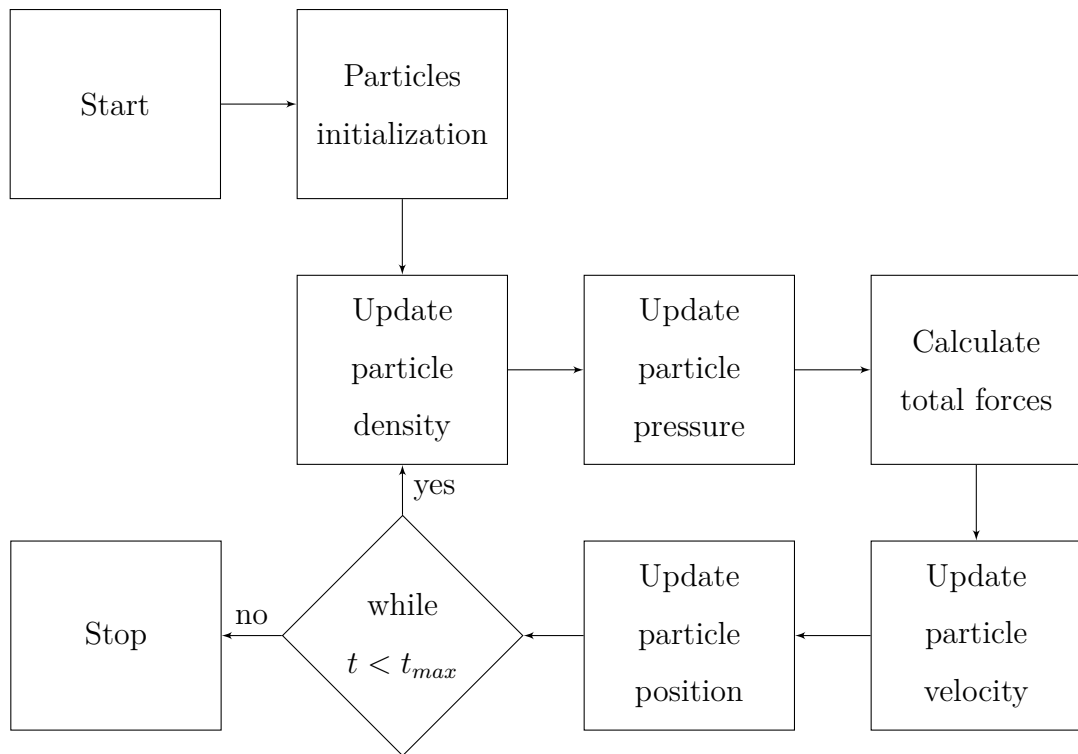
Figure 1.2: Diagram of procedure for solving governing equations

The outcome position is plotted on 2- and 3-dimensions. The status, receding and advancing angles of the droplet are measured and compared with the experimental data [20].

1.4   Literature Review

Review on droplet motion on vertical plane

The profile of static droplet on vertical surface was studied by Merte and Yamali [10] using variational calculus technique to obtain the equation of surface of the droplet as the function of advancing angle, θ_A, by minimizing total energy. The departure size of droplet, where surface tension can no longer support the gravitational force is determined as well.

Milinazzo and Shinbrot [11] presented the dimensionless number called Bond number, Bo, which is a ratio of the gravitational force to the surface tension force on their numerical study

$$Bo = \frac{\rho g D^2}{\sigma},$$

where ρ is density of the fluid, g is acceleration of gravity, D is the drop's diameter, and σ is the surface tension of liquid-gas interface. They assumed the droplet has a fixed area while the Bond number is increasing from zero. They found that increasing the Bond number is related to an increase in the inclination angle of the plane.

The volume of fluid-continuous surface force (VOF-CSF) model with the contact angles [20] is used to predict the droplet motion on vertical surface under gravity, surface tension and airflow force in tube-finned heat exchangers and to optimize the fin surface as well. The outcome is verified by the experimental data in term of receding angle. In the experiment, certain quantity droplets are given from micro-liter syringe, then the high-speed camera is used to capture the profile of droplet. After that the contact angle is measured by the image processing software.

Review on surface tension model combined with SPH method

Nugent and Posch [17] applied the cohesive pressure of Van der Waal (VdW) equation of state giving the force acting between particles to model the surface tension in 2-dimensional SPH simulation. But it was necessary to increase the

support domain of kernel function twice for rising force. That caused an increase of the computational time from range of computational domain is increasing.

Morris [16] and Das and Das [4] have integrated the continuum surface force (CSF) [2] into SPH scheme. In CSF method, the surface tension force is calculated from the interfacial curvature of the fluids. The curvature is defined as how fast the tangential vector which corresponds to the normal vector, $\mathbf{n}$, rotates through the arc length. Brackbill et. al. [2] proposed the approximation of the curvature, κ, by using the divergence of normal vector expressed by

$$\kappa = -\nabla \cdot \mathbf{n}.$$

This method provides an accurate approximation for the surface tension. However, it involves complex calculation which leads to inefficient computational time.

Tartakovsky and Meakin [19] simulated the surface tension by pairwise fluid-fluid fluid-solid particle-particle interactions along with standard SPH equations. The idea is similar to Nugent and Porch [17] but need not to expand the computational domain. We have employed the Tartakovsky and Meakin's model [19] as the burdensome of evaluation of curvature is lacking.

1.5   Outline of the Thesis

This thesis is divided into 5 chapters structured as follows. Chapter 1 is an introduction of this work including the objectives, literature reviews, method used in this work and the outline of this thesis. Chapter 2 discussed about the governing equations that explain this phenomenon and its derivation briefly. Chapter 3 presents the details on the Smoothed Particle Hydrodynamics (SPH) which is the main method used and its implementation on the governing equations. Some numerical aspects and computational strategies on neighbor searching algorithm are discussed. Chapter 4 provides the simulation results in 2- and 3-dimensional systems with validation by comparing the numerical results with the experimental data given by Zhuang et. al. [20]. Chapter 5, the last chapter, gives the conclusions of this work and the plan for future works.

CHAPTER II
GOVERNING EQUATIONS

In this chapter, we explain the derivation of governing equations which describe the motion of the droplet. To describe the fluid motion, there are 2 approaches commonly used. One is the Eulerian description that focusing the fluid motion on specific location which the fluid moves through it as time passes. Another is the Lagrangian description that observing the infinitesimal fluid element as it moves through space and time. Even a way of consideration is different, both of them can lead to the equations that follow the laws of physics. Since the SPH method, which the particles carry the physical quantities and move with the motion of fluid is similar to a way of Lagrangian description. The governing equations will be derived in Lagrangian form.
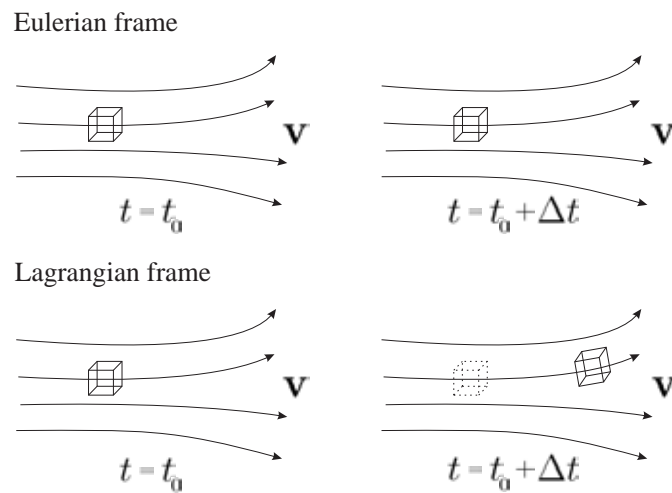
Figure 2.1: Concept of Eulerian and Lagragian description

2.1 Material Derivative

It is sometimes called *substantial derivative*, representing the time rate of change of some physical quantity of the infinitesimal fluid element. It can serve as a link between Eulerian description and Lagrangian description. Its operator can be expressed by

$$\frac{D}{Dt} = \frac{\partial}{\partial t} + (\mathbf{v} \cdot \nabla),$$

where $\mathbf{v} = (u, v, w)$ is the velocity field in x-, y-, and z- directions respectively. It consists of two parts: $\frac{\partial}{\partial t}$ is called the local derivative, which is physically a time rate of change at a fixed point, and $(\mathbf{v} \cdot \nabla)$ is the convective derivative which is physically a change due to the movement of the fluid element from one location to another. A material derivative is a total derivative of any function ψ of space and time

$$\begin{aligned}
\frac{d}{dt}\psi(x, y, z, t) &= \frac{\partial\psi}{\partial t} + \frac{\partial\psi}{\partial x}\frac{dx}{dt} + \frac{\partial\psi}{\partial y}\frac{dy}{dt} + \frac{\partial\psi}{\partial z}\frac{dz}{dt} \\
&= \frac{\partial\psi}{\partial t} + u\frac{\partial\psi}{\partial x} + v\frac{\partial\psi}{\partial y} + w\frac{\partial\psi}{\partial z} \\
&= \left(\frac{\partial}{\partial t} + \mathbf{v} \cdot \nabla\right)\psi \\
&= \frac{D\psi}{Dt}.
\end{aligned}$$

One useful expression $\nabla \cdot \mathbf{v}$ which is the time rate of change of the volume of an infinitesimal moving fluid element per unit volume is expressed by [8]

$$\nabla \cdot \mathbf{v} = \frac{1}{\delta V}\frac{D(\delta V)}{Dt}, \tag{2.1}$$

where δV is the volume of an infinitesimal moving fluid element.

2.2 Continuity Equation

For an infinitesimal fluid element with a volume δV, the relation between a volume and a mass δm is given by

$$\delta m = \rho \delta V.$$

Since the continuity equation is based on the law of conservation of mass, the time rate of change is zero. We get

$$
\begin{aligned}
0 &= \frac{D(\delta m)}{Dt} \\
&= \frac{D(\rho \delta V)}{Dt} \\
&= (\delta V)\frac{D\rho}{Dt} + \rho\frac{D(\delta V)}{Dt} \\
&= \frac{D\rho}{Dt} + \rho\left(\frac{1}{\delta V}\frac{D(\delta V)}{Dt}\right).
\end{aligned}
$$

Since $\nabla \cdot \mathbf{v} = \dfrac{1}{\delta V}\dfrac{D(\delta V)}{Dt}$ from (2.1), the continuity equation in Lagrangian form is obtained as

$$
\frac{D\rho}{Dt} = -\rho\left(\nabla \cdot \mathbf{v}\right) \tag{2.2}
$$

2.3 Momentum Equation

The momentum equation follows the Newton's second law. When applied to an infinitesimal fluid element, the net force equals to its mass times the acceleration of the element. In an inviscid fluid case, the total forces acting on the element are only pressure force and body force. Figure 2.2 explains how the pressure force
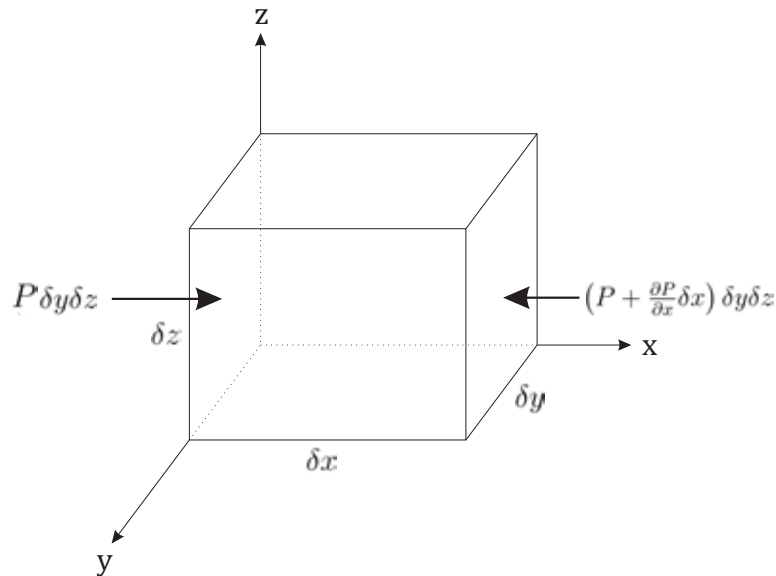
Figure 2.2: The pressure forces acting on an infinitesimal fluid element in x-axis

acts on the element in the x-axis. Consider the pressure force acting on the left

and right faces of the element, the force $P\,\delta y\delta z$ and $\left(P + \frac{\partial P}{\partial x}\delta x\right)\delta y\delta z$ press inward on the element in the x and $-x$ directions, respectively. Given the volume of the element is $\delta V = \delta x\delta y\delta z$. Let us denoted the body force by $\mathbf{F}_B = \rho(\delta x\delta y\delta z)\mathbf{f}$, where $\mathbf{f} = (f_1, f_2, f_3)$ is a body force per unit mass. The total forces acting on an infinitesimal fluid element on x-axis are

$$
\begin{aligned}
F_x &= \left(P - \left(P + \frac{\partial P}{\partial x}\delta x\right)\right)\delta y\delta z \ + \ \rho(\delta x\delta y\delta z)f_1, \\
\delta m\, a_x &= -\frac{\partial P}{\partial x}\delta x\delta y\delta z \ + \ \rho f_1 \delta x\delta y\delta z, \\
\rho(\delta x\delta y\delta z)\, a_x &= \left(-\frac{\partial P}{\partial x} + \rho f_1\right)(\delta x\delta y\delta z), \\
\rho a_x &= -\frac{\partial P}{\partial x} + \rho f_1.
\end{aligned}
$$

Recalling that we are following a moving element, a_x is given by the material derivative $\frac{Du}{Dt}$. Following the same procedure for y- and z-axes. Hence, we obtain

$$
\begin{aligned}
\rho\frac{Du}{Dt} &= -\frac{\partial P}{\partial x} + \rho f_1, \\
\rho\frac{Dv}{Dt} &= -\frac{\partial P}{\partial y} + \rho f_2, \\
\rho\frac{Dw}{Dt} &= -\frac{\partial P}{\partial z} + \rho f_3.
\end{aligned}
$$

Finally, the momentum equation in the Lagrangian form is arrived as

$$
\rho\frac{D\mathbf{v}}{Dt} = -\nabla P + \rho\mathbf{f}. \tag{2.3}
$$

2.4   Surface Tension

We can see in a practical life that the effect of surface tension such as small insects can walk on the water and the needle can be floated on the water, even using the detergents for washing is also the effect of the surface tension. In fluid dynamics, there exists a dimensionless number which represents the importance of surface tension force compared to body force which is usually the gravity called Bond number, Bo, that is defined by

$$
Bo = \frac{\rho g D^2}{\sigma},
$$

where ρ is density of the fluid, g is acceleration of gravity, D is the drop's diameter, and σ is the surface tension of liquid-gas interface. Higher the Bond number, less the effect of surface tension. This means the gravity has more influence. A low number (normally, less than 1) illustrates that the surface tension force is governed.

The surface tension is actually not a part of the governing equations, but it plays a significant role to make the droplet keeps the shape and is able to be hanged on the wall. A water molecule in the droplet share the cohesive forces between itself and neighbor molecules, whereas the molecules at the surface do not have the neighbor molecules all sides of them, resulting the net force is not zero. The force acts normal to the surface in inward (to the fluid) direction, which binds the fluid surface together and flatten the surface curvature by minimizing the surface area. Thus, the droplet tends to evolve into a spherical shape ([6] and [7]).

Unlike the cohesion, if a water molecule is attracted to other material, the force called "adhesion" is occured. It provides water is attracted by other material. In the small droplet that is hanged on the surface. Adhesive force acting between water molecule and surface is strong enough to withstand the effect from gravitatonal force. An example of cohesion and adhesion on water droplet in nature is shown in Figure 2.3. The adhesion makes water droplets resting on the Hibiscus flower in spherical shape by the effect of cohesion.

Figure 2.3: An example in nature. The water droplets rest on the Hibiscus flower [18]

CHAPTER III

SMOOTHED PARTICLE HYDRODYNAMICS

This chapter, we talk about the main method used to solve our main problem. Smoothed Particle Hydrodynamics (SPH) is a meshfree numerical method which was first introduced to solve an astrophysical simulation by Lucy [9] based on Lagrangian formulation but nowadays it widely used to solve the hydrodynamics problem. It is also preferable for free and moving surface, large deformation and complex mesh generation problems which are difficult to apply in grid-based method. With this method, the fluid is discretized into a set of points, referred as "particle", in which each particle carries its physical quantities, e.g. mass, position, velocity etc.

3.1 SPH Formulation

In an idea of SPH approximation, a general field variable A is approximated through integral interpolant over all the space Ω as in the following

$$A(\boldsymbol{r}) = \int_{\Omega} A(\boldsymbol{r}')\, \delta(\boldsymbol{r} - \boldsymbol{r}')\, d\boldsymbol{r}', \tag{3.1}$$

where $\boldsymbol{r}$ is a position vector in Ω, and δ is a Dirac delta function given by

$$\delta(\boldsymbol{r}) = \begin{cases} \infty, & \boldsymbol{r} = \boldsymbol{r}', \\ 0, & \boldsymbol{r} \neq \boldsymbol{r}'. \end{cases} \tag{3.2}$$

The SPH idea is using the weight function $W(\boldsymbol{r} - \boldsymbol{r}', h)$ (the details are in Section 3.2) which is usually called *kernel function* or *smoothing function*, where h is the smoothing length that stands for influence or support area of weight function W to replace the Dirac delta function above. Hence, (3.1) becomes

$$A(\boldsymbol{r}) = \int_{\Omega} A(\boldsymbol{r}')\, W(\boldsymbol{r} - \boldsymbol{r}', h)\, d\boldsymbol{r}'. \tag{3.3}$$

As for the first derivative of A at position $\boldsymbol{r}$, denoted by $\nabla_{\boldsymbol{r}} A(\boldsymbol{r})$, substituting $\nabla_{\boldsymbol{r}} A(\boldsymbol{r})$ into (3.3), we have

$$\nabla_{\boldsymbol{r}} A(\boldsymbol{r}) = \int_{\Omega} [\nabla_{\boldsymbol{r}'} A(\boldsymbol{r}')]\, W(\boldsymbol{r} - \boldsymbol{r}', h)\, d\boldsymbol{r}'. \tag{3.4}$$

Using integration by parts on higher dimension, we obtain

$$\begin{aligned} \nabla_{\boldsymbol{r}} A(\boldsymbol{r}) &= \int_{S} A(\boldsymbol{r}')\, W(\boldsymbol{r} - \boldsymbol{r}', h)\, \mathbf{n}\, dS \\ &\quad - \int_{\Omega} A(\boldsymbol{r}')\, \nabla_{\boldsymbol{r}'} W(\boldsymbol{r} - \boldsymbol{r}', h)\, d\boldsymbol{r}', \end{aligned} \tag{3.5}$$

where S is the surface of Ω and $\mathbf{n}$ is the unit outward surface normal to S. Since the smoothing function W has a compact support (see Section 3.2), the value of W on the surface S of Ω is zero, it gives the first term on RHS of (3.5) becomes zero. Therefore, the approximation for derivative, the equation (3.4) can be written as

$$\nabla_{\boldsymbol{r}} A(\boldsymbol{r}) = -\int_{\Omega} A(\boldsymbol{r}')\, \nabla_{\boldsymbol{r}'} W(\boldsymbol{r} - \boldsymbol{r}', h)\, d\boldsymbol{r}'. \tag{3.6}$$

Moreover, we obtain

$$\nabla_{\boldsymbol{r}} \cdot A(\boldsymbol{r}) = -\int_{\Omega} A(\boldsymbol{r}')\, \cdot \nabla_{\boldsymbol{r}'} W(\boldsymbol{r} - \boldsymbol{r}', h)\, d\boldsymbol{r}'. \tag{3.7}$$

In SPH, the fluid is represented as a finite number of particles. Then, we can rewrite (3.3) into discretized form by replacing integral interpolant by a summation interpolant and $d\boldsymbol{r}'$ by approximation of particle's volume $V_j = \frac{m_j}{\rho_j}$, where m_j and ρ_j are the mass and density of particle j, respectively. The value of A at $\boldsymbol{r}_i$ is as follows

$$A(\boldsymbol{r}_i) = \sum_{j} m_j \frac{A_j}{\rho_j} W_{ij}, \tag{3.8}$$

where $W_{ij} = W(\boldsymbol{r}_i - \boldsymbol{r}_j, h) = W(|\boldsymbol{r}_i - \boldsymbol{r}_j|, h)$ and j is referred to all neighbour particle of particle i. Thus, we obtain the approximation of any continuous field variable. In the same procedure, the approximation of a derivative at position $\boldsymbol{r}_i$, $\nabla_i A(\boldsymbol{r}_i)$, can be expressed as

$$\nabla_i A(\boldsymbol{r}_i) = -\sum_{j} m_j \frac{A_j}{\rho_j} \nabla_j W_{ij}, \tag{3.9}$$

$$\nabla_i \cdot A(\boldsymbol{r}_i) = -\sum_{j} m_j \frac{A_j}{\rho_j} \cdot \nabla_j W_{ij}. \tag{3.10}$$
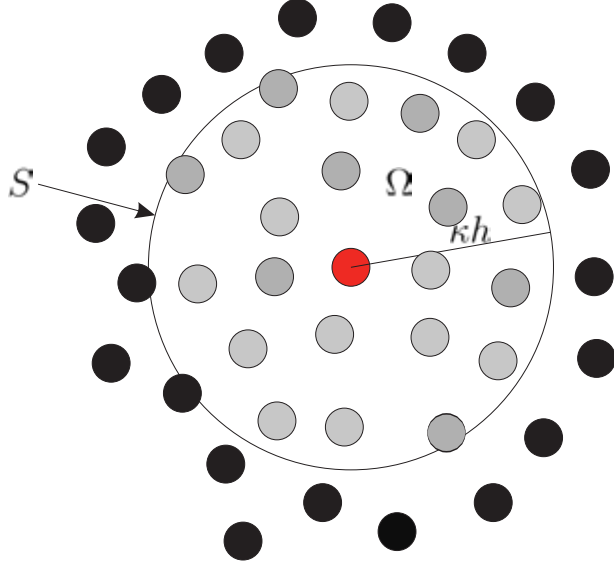
Figure 3.1: The circular support domain of kernel function W with radius κh for particle i (red) with neighbor particles (gray)

Noting that, the gradient $\nabla_j W_{ij}$ in the above equation is taken with respect to particle j. It should be noted that the negative sign is removed if we replace $\nabla_j W_{ij}$ by $\nabla_i W_{ij}$. Let us denote $\nabla_i W_{ij} = \frac{r_i - r_j}{|r_i - r_j|} \frac{\partial W_{ij}}{\partial |r_i - r_j|}$. Hence, (3.9) becomes

$$\nabla_i A(\boldsymbol{r}_i) = \sum_j m_j \frac{A_j}{\rho_j} \nabla_i W_{ij}, \tag{3.11}$$

$$\nabla_i \cdot A(\boldsymbol{r}_i) = \sum_j m_j \frac{A_j}{\rho_j} \cdot \nabla_i W_{ij}. \tag{3.12}$$

Now, we have shown the discretized form of integral representation of a function and also its derivative by using the summation over all particles in the support domain of the kernel function which is a key factor influencing the accuracy of SPH method. The next section describes about the kernel function and its properties.

3.2 Kernel Function

In the SPH method, the kernel function plays an important role to perform the function approximation. It determines the interpolation pattern and also the influencing area of the particle. The properties of kernel function are summarized as follows:

- (*normalization condition* or sometimes called *unity condition*) the integral of W over the space is unity

$$\int_\Omega W(\boldsymbol{r} - \boldsymbol{r}', h)\, d\boldsymbol{r}' = 1;$$

- (*Dirac delta property*) the limit for h approach to zero of W is the Dirac delta function

$$\lim_{h \to 0} W(\boldsymbol{r} - \boldsymbol{r}', h) = \delta(\boldsymbol{r} - \boldsymbol{r}');$$

- (*compact condition*)

$$W(\boldsymbol{r} - \boldsymbol{r}', h) = 0 \qquad \text{when } |\boldsymbol{r} - \boldsymbol{r}'| > \kappa h,$$

where κ is a constant determining the support domain of the smoothing function W. It can be called that the value of W is zero outside the support domain of W;

- (*symmetric property*) the smoothing function W should be an even function. It means the particles from the same distance gives the equal effect on a given particle

$$W(\boldsymbol{r} - \boldsymbol{r}', h) = W(|\boldsymbol{r} - \boldsymbol{r}'|, h) = W(\boldsymbol{r}' - \boldsymbol{r}, h).$$

From the above properties, there are many kinds of kernel functions which have been used in many papers on SPH. In [16], they found that a spline function of at least fourth order presents an accurate result of free surfaces. We thus used a quintic spline function as a kernel function in this work.

$$W(\boldsymbol{r}, h) = \begin{cases} \alpha\left(\left(3 - \dfrac{3|\boldsymbol{r}|}{h}\right)^5 - 6\left(2 - \dfrac{3|\boldsymbol{r}|}{h}\right)^5 + 15\left(1 - \dfrac{3|\boldsymbol{r}|}{h}\right)^5\right), & 0 \le |\boldsymbol{r}| < \dfrac{h}{3}, \\[2ex] \alpha\left(\left(3 - \dfrac{3|\boldsymbol{r}|}{h}\right)^5 - 6\left(2 - \dfrac{3|\boldsymbol{r}|}{h}\right)^5\right), & \dfrac{h}{3} \le |\boldsymbol{r}| < \dfrac{2h}{3}, \\[2ex] \alpha\left(\left(3 - \dfrac{3|\boldsymbol{r}|}{h}\right)^5\right), & \dfrac{2h}{3} \le |\boldsymbol{r}| < h, \\[2ex] 0, & |\boldsymbol{r}| > h, \end{cases}$$

$$\tag{3.13}$$

where $\alpha = 63/478\pi h^2$ and $9/40\pi h^3$ for the 2- and 3-spatial dimensions, respectively.
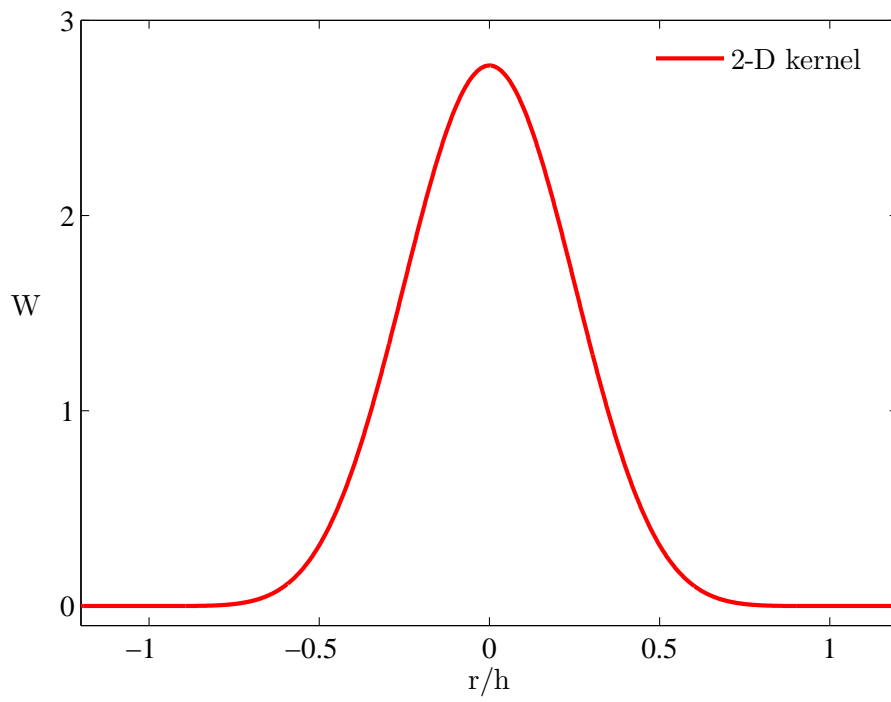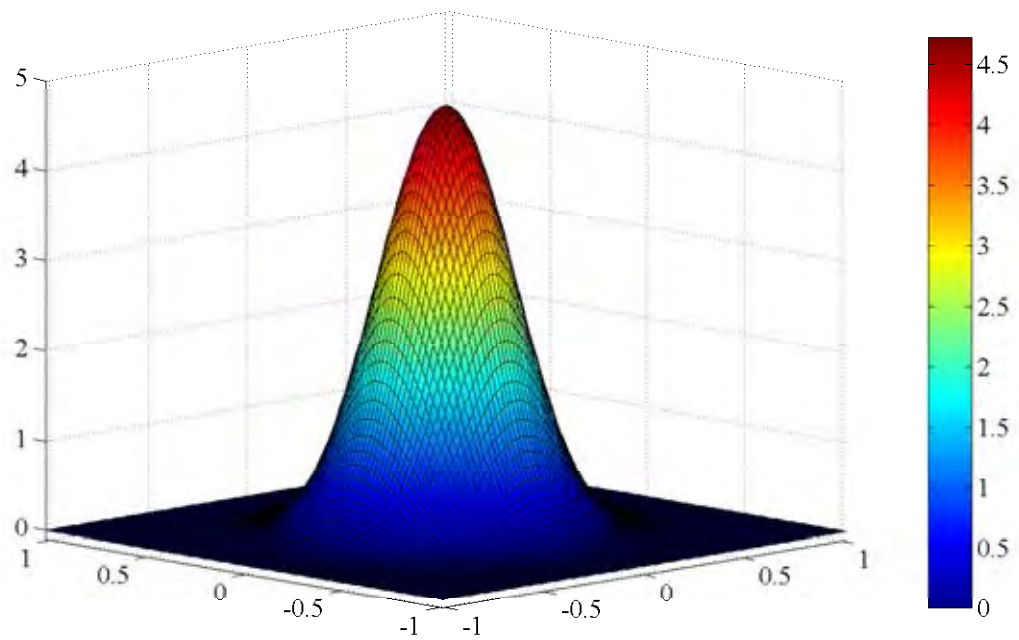
Figure 3.2: 2-D kernel used in this work

Figure 3.3: 3-D kernel used in this work

From Figure 3.2 - 3.3, it is obvious that this kernel function has symmetric property and compact condition with $\kappa = 1$. Also it is easy to see that $\lim\limits_{h \to 0} W(\boldsymbol{r}, h) = \infty$ if $|\boldsymbol{r}| = 0$ and $\lim\limits_{h \to 0} W(\boldsymbol{r}, h) = 0$ if $|\boldsymbol{r}| > 0$. Then, it holds the Dirac delta property. The last condition to be checked is unity condition. For 2-dimensional kernel function,

$$
\begin{aligned}
\int_{\Omega} W(\boldsymbol{r}, h)\, d\Omega \;=\;& \alpha \int_{0}^{2\pi} \int_{0}^{h} \left[\left(3 - \frac{3|\boldsymbol{r}|}{h} \right)^5 \right] \boldsymbol{r}\, d\boldsymbol{r}\, d\theta \\
&+ \alpha \int_{0}^{2\pi} \int_{0}^{2h/3} \left[-6 \left(2 - \frac{3|\boldsymbol{r}|}{h} \right)^5 \right] \boldsymbol{r}\, d\boldsymbol{r}\, d\theta \\
&+ \alpha \int_{0}^{2\pi} \int_{0}^{h/3} \left[15 \left(1 - \frac{3|\boldsymbol{r}|}{h} \right)^5 \right] \boldsymbol{r}\, d\boldsymbol{r}\, d\theta \\
=\;& \alpha \int_{0}^{2\pi} \left(\frac{81h^2}{14} \right) d\theta + \alpha \int_{0}^{2\pi} \left(\frac{-128h^2}{63} \right) d\theta + \alpha \int_{0}^{2\pi} \left(\frac{5h^2}{126} \right) d\theta \\
=\;& \alpha \left(\frac{81\pi h^2}{7} \right) + \alpha \left(\frac{-256\pi h^2}{63} \right) + \alpha \left(\frac{5\pi h^2}{63} \right) \\
=\;& \alpha \left(\frac{478\pi h^2}{63} \right) = 1.
\end{aligned}
$$

For 3-dimensional kernel function,

$$
\begin{aligned}
\int_{\Omega} W(\boldsymbol{r}, h)\, d\Omega \;=\;& \alpha \int_{0}^{2\pi} \int_{0}^{\pi} \int_{0}^{h} \left[\left(3 - \frac{3|\boldsymbol{r}|}{h} \right)^5 \right] \boldsymbol{r}^2 \sin\phi\, d\boldsymbol{r}\, d\phi\, d\theta \\
&+ \alpha \int_{0}^{2\pi} \int_{0}^{\pi} \int_{0}^{2h/3} \left[-6 \left(2 - \frac{3|\boldsymbol{r}|}{h} \right)^5 \right] \boldsymbol{r}^2 \sin\phi\, d\boldsymbol{r}\, d\phi\, d\theta \\
&+ \alpha \int_{0}^{2\pi} \int_{0}^{\pi} \int_{0}^{h/3} \left[15 \left(1 - \frac{3|\boldsymbol{r}|}{h} \right)^5 \right] \boldsymbol{r}^2 \sin\phi\, d\boldsymbol{r}\, d\phi\, d\theta \\
=\;& \alpha \int_{0}^{2\pi} \int_{0}^{\pi} \left(\frac{81h^3}{56} - \frac{64h^3}{189} + \frac{5h^3}{1512} \right) \sin\phi\, d\phi\, d\theta \\
=\;& \alpha \left(\frac{81h^3}{8} - \frac{256h^3}{189} + \frac{5h^3}{378} \right) \\
=\;& \alpha \left(\frac{40\pi h^3}{9} \right) = 1
\end{aligned}
$$

This shows that the kernel function has a unity condition.

3.3   SPH Scheme on Governing Equations

This section considers applying the SPH approximation that we have discussed in the previous section to the governing equations to obtain the numerical scheme for our problem.

3.3.1   Continuity Equation

To approximate the continuity equation, (2.2), using SPH approximation, we rewrite (2.2) in the form of product rule of $\rho\,(\nabla \cdot \mathbf{v})$

$$\frac{D\rho}{Dt} \;=\; \mathbf{v} \cdot (\nabla \rho) - \nabla \cdot (\rho \mathbf{v}).$$

Substituting $\mathbf{v} \cdot (\nabla \rho)$ and $\nabla \cdot (\rho \mathbf{v})$ into (3.11) and (3.12), we obtain

$$\begin{aligned}
\frac{D\rho_i}{Dt} &= \sum_j m_j \mathbf{v}_i \cdot \nabla W_{ij} - \sum_j m_j \mathbf{v}_j \cdot \nabla W_{ij} \\
&= \sum_j m_j (\mathbf{v}_i - \mathbf{v}_j) \cdot \nabla W_{ij}.
\end{aligned} \tag{3.14}$$

Another approximation of density of particle is to substitute ρ into (3.8), we have

$$\rho_i \;=\; \sum_j m_j \frac{\rho_j}{\rho_j} W_{ij} \;=\; \sum_j m_j W_{ij}. \tag{3.15}$$

For simplicity, in this work, we use (3.15) to approximate the density of the particle.

3.3.2   Momentum Equation

Considering the momentum equation, (2.3), with only the gravitational force as the external forces, we have

$$\frac{D\mathbf{v}}{Dt} \;=\; -\frac{1}{\rho}\nabla P \,+\, \mathbf{g} \tag{3.16}$$

where $\mathbf{g}$ is the gravitation force per unit mass. There are many formulae that can be used to approximate pressure gradient, ∇P. The simplest is directly substituting the pressure gradient, ∇P, into (3.9), we get

$$\frac{D\mathbf{v}_i}{Dt} \;=\; -\frac{1}{\rho_i}\sum_j m_j \frac{P_j}{\rho_j}\nabla W_{ij} \,+\, \mathbf{g}. \tag{3.17}$$

However, it is not a good approximation. Since considering any pairwise interaction between particle i and j, we see that the pressure force acting on particle i is from the information of particle j, and vice versa. That means the amount of force received by particle j due to particle i is not the same as the amount of force received by particle i due to particle j. It provides the total system force is not zero. Then, the scheme that fixed this disadvantage and conserved the momentum is proposed by Monaghan [13]. Rewriting the pressure gradient term by

$$\frac{\nabla P}{\rho} = \nabla \left(\frac{P}{\rho} \right) + \frac{P}{\rho^2} \nabla \rho.$$

Hence, the momentum equation, (3.16), becomes

$$
\begin{aligned}
\frac{D\mathbf{v}_i}{dt} &= -\left(\sum_j \frac{m_j}{\rho_j} \left(\frac{P_j}{\rho_j} \right) \nabla W_{ij} + \frac{P_i}{\rho_i^2} \sum_j m_j \frac{\rho_j}{\rho_j} \nabla W_{ij} \right) + \mathbf{g} \\
&= -\left(\sum_j m_j \left(\frac{P_i}{\rho_i^2} + \frac{P_j}{\rho_j^2} \right) \nabla W_{ij} \right) + \mathbf{g}
\end{aligned}
\tag{3.18}
$$

and we used this scheme in this work. Anyhow, this is not the final scheme. The artificial viscosity and the surface tension force will be added. Their details will be discussed in the next section.

3.4 Numerical Aspects

3.4.1 Pressure

In the momentum equation, (2.3), the value of pressure is needed in order to calculate the acceleration. The Tait's equation of state [1] used in this thesis is

$$P = B \left(\left(\frac{\rho}{\rho_0} \right)^\gamma - 1 \right), \tag{3.19}$$

where ρ_0 is a reference density (in the case of water, $\rho_0 = 1000 \ kg/m^3$), γ shall be 7 for water-like fluid case, and B is a constant standing for the relation between the speed of sound, c, at a reference density [14]

$$B = \frac{c^2 \rho_0}{\gamma}.$$

3.4.2   Artificial Viscosity

The artificial viscosity is considered to be added to the momentum equation, (3.18), to reduce the unphysical oscillations around the shocked regions which have a large amount of difference of pressure and also to prevent unphysical particles' penetration when approaching each other [8] and to improve the code stability. The artificial viscosity scheme we used is one of the most popular in SPH simulations proposed by [13] written as

$$\Pi_{ij} = \begin{cases} \dfrac{-\alpha_\Pi\, c\, \phi_{ij}\, +\, \beta_\Pi\, \phi_{ij}^2}{\bar{\rho}_{ij}}, & \mathbf{v}_{ij}\cdot\boldsymbol{r}_{ij} < 0, \\[2mm] 0, & \mathbf{v}_{ij}\cdot\boldsymbol{r}_{ij} \geq 0. \end{cases} \tag{3.20}$$

and

$$\phi_{ij} \;=\; \frac{h\,\mathbf{v}_{ij}\cdot\boldsymbol{r}_{ij}}{|\boldsymbol{r}_{ij}|^2 + 0.01h^2},$$

$$\bar{\rho}_{ij} = \frac{1}{2}(\rho_i + \rho_j), \qquad \mathbf{v}_{ij} = \mathbf{v}_i - \mathbf{v}_j, \qquad \boldsymbol{r}_{ij} = \boldsymbol{r}_i - \boldsymbol{r}_j,$$

where c is a speed of sound, α_Π and β_Π are constants usually set around 1 [12]

3.4.3   Surface Tension

As we know that surface tension force is an external force applying to the surface of fluid which is normally the boundary condition of the Navier-Stokes equation. In SPH, it can be considered that the surface tension force is acting on the surface particles. However, to find the surface particles is quite more complex and gives an increase in the computational time. Thereby, we employ the Tartakovsky and Meakin model [19] which considers the surface tension force as the partice-particle interactions added to momentum equation that we have described above. Let us denote $\mathbf{F}_{ij}$ be the force acting between particles i and j written as

$$\mathbf{F}_{ij} = \begin{cases} s_{ij}\cos\left(\dfrac{0.5\pi}{h}|\boldsymbol{r}_j - \boldsymbol{r}_i|\right)\dfrac{\boldsymbol{r}_j - \boldsymbol{r}_i}{|\boldsymbol{r}_j - \boldsymbol{r}_i|}, & |\boldsymbol{r}_j - \boldsymbol{r}_i| \leq h, \\[3mm] 0, & |\boldsymbol{r}_j - \boldsymbol{r}_i| > h. \end{cases} \tag{3.21}$$

where s_{ij} is the strength of the force acting between the particles i and j. The value is different for fluid-fluid, fluid-wetted solid and fluid-not wetted solid interactions. The total forces acting on any particle i can be expressed as

$$\mathbf{F}_i = \sum_j \mathbf{F}_{ij}.$$

We see that $\mathbf{F}_{ij} = -\mathbf{F}_{ji}$, hence, this kind of particle-particle interactions conserve the momentum. Although this added force is not only acting on the surface particles, the total force acting on the particle is nonzero only near the fluid surfaces, fluid-solid interfaces. The risen force creates surface tension. Let us denote $\frac{\mathbf{F}_i}{m_i}$ be the acceleration comes from the surface tension force and put it and also the artificial viscosity Π_{ij} into the momentum equation, (3.18). We eventually obtain the final scheme on momentum equation

$$\frac{D\mathbf{v}_i}{Dt} = -\left(\sum_j m_j \left(\frac{P_i}{\rho_i^2} + \frac{P_j}{\rho_j^2} + \Pi_{ij} \right) \nabla W_{ij} \right) + \mathbf{g} + \frac{\mathbf{F}_i}{m_i}. \tag{3.22}$$

3.4.4 Neighbor Searching Algorithm

In SPH method, the particles need to check their neighbor particles that interact with itself at every time step which causes a great amount of computational time. In the followings, two techniques will be introduced

All Particles Search

The simplest algorithm used to find the neighbor particles. To find out the particles which are in the support domain of the current particle, it checks the distance between itself and whole particles in the domain. This means that, if the number of particles in the whole domain is N, the time complexity of this algorithm is $O(N^2)$. The pseudo-code is presented below

```
for(int i=0; i<N ; i++)
  for(int j=0; j<N ; j++)
    checking_distance(i, j);.
```

We see that the distance between particle i and j is symmetric, the value of smoothing function W between couple of particles i and j are the same, ($W_{ij} = W_{ji}$). Thus, no need to compute the value of smoothing function twice, we can reduce the computational time by symmetrized the previous algorithm as follows

```
for(int i=0; i<N ; i++)
  for(int j=i+1; j<N ; j++)
    checking_distance(i, j);.
```
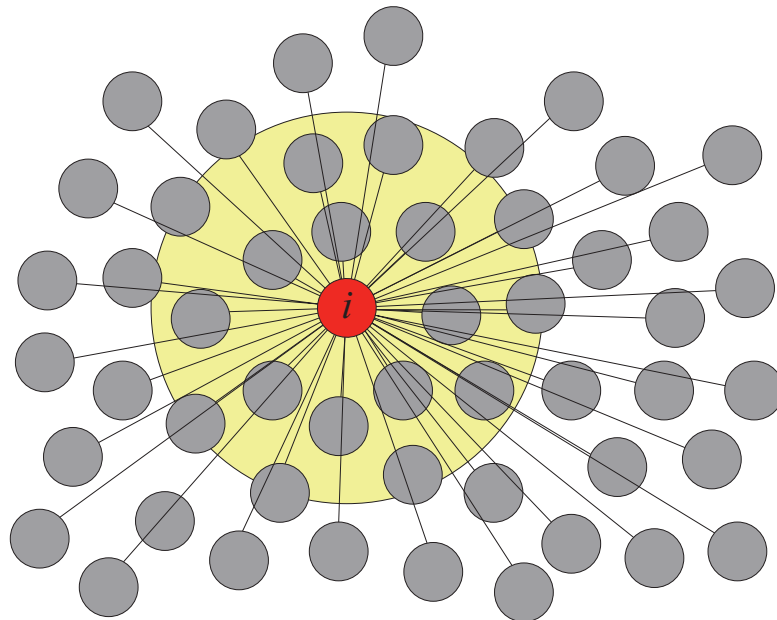

Figure 3.4: The scheme for all particles searching.

Linked-list Algorithm

Due to checking all the particles suffers a long computational time. To develop the method, several techniques were proposed. One of them is called 'linked-list method'. The main idea is to overlay the cell on the whole domain which its size equals to support radius of kernel function κh. Seeing that all particles are assigned into a cell, then the neighbor particles of each particle are placed in the same grid and its adjacent cells. It provides the cells to checked are only 3, 9 or 27 cells for 1-, 2- or 3-dimensions, respectively.
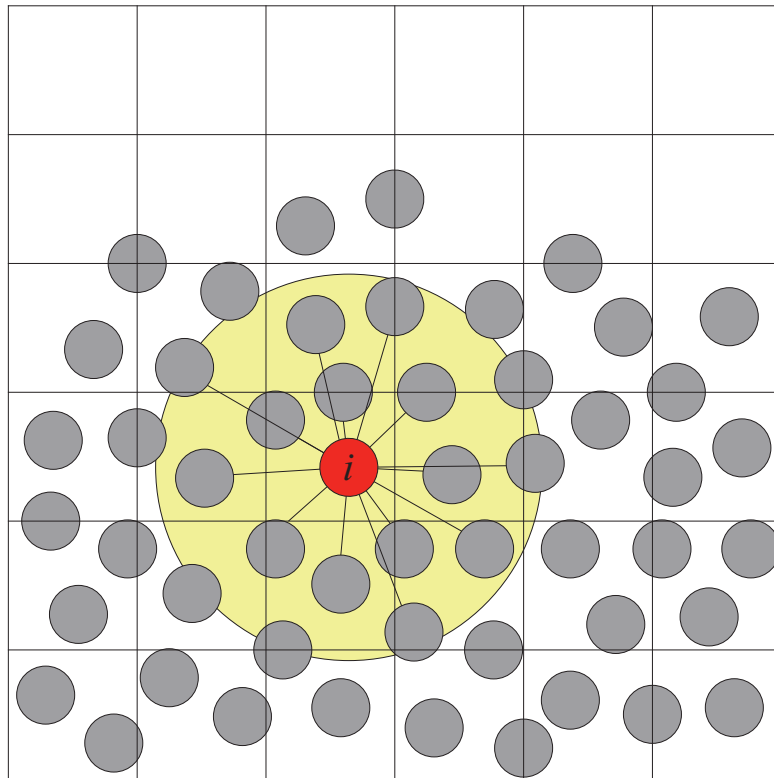
Figure 3.5: The scheme for linked-list method. Overlaying the cell on the domain and the particles are assigned into the cell

From data structure point of view, each cell can only save one particle or no particle contained in that cell. Then, each particle saves the information of a next particle arriving at its, same cell as a chain. Using this method, neighbor searching algorithm can be work in $O(kN)$, where k is proportional to the average number of neighbors. That greatly improves the neighbor searching algorithm. How to construct the linked-list of all particles is presented in pseudo-code below

```
for (int i=0; i<N ; i++){
  int gn = finding_grid_number[i];
  if (grid[gn] == -1)
    grid[gn] = i;
  else {
    int j = grid[gn];
    while (next[j] != -1){
      j = next[j];
```

```
    }
    next[j] = i
  }
}.
```

The weak point of this method is when the smoothing length is not a constant, the constructed cells may not be fine for every particle. Hence, the efficacy may be less.

(a) Empty cell   (b) Occupied cell

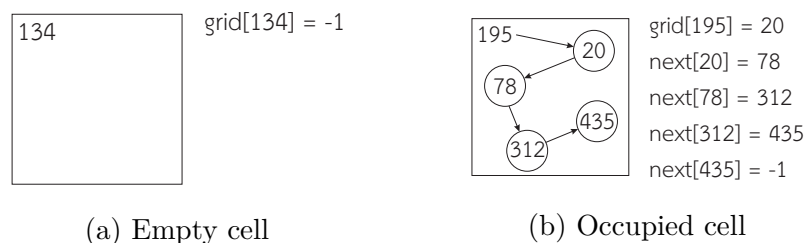Figure 3.6: Example of the handling in empty cell (cell 134) and occupied cell (cell 195 with particle 20, 78, 312 and 435) on allocation of the next particle (-1 is denoted that there is no next particle).

3.4.5   Wall Boundary

In this work, the rigid boundary method was applied because of its simplicity for implementing when we consider the wall boundary. We add the rigid boundary particles on the boundary as a wall. The wall particles interact with another particles same as the normal fluid particles. However, in the time integration step, they will not be updated the position.

According to the force that acting between the fluid-solid interactions is different for fluid-wetted particles and fluid-not wetted particles (as we have discussed in section 3.4.3), the boundary particles will be detected whether it is wetted or not wetted particles. As the by-product from linked-list method, we already assigned the particles into the constructed cells, the boundary particles as well. First, we impose all boundary particles to be not wetted. For each time step, if we detect a particle placed in a cell that is contiguous with boundary cell, we assign

the boundary particles in that contiguous cell to be wetted under the assumption that the particles being wetted once, are always wet.

3.4.6 Numerical Time Integration

The particle accelereation is computed by (3.22). In order to update the new particle velocity and position, we integrate the acceleration numerically. In this research, we employ the leap-frog integration scheme which gives the better accuracy than Euler's scheme and lack of complexity. To update the particle position at a new time step, it uses the information of velocity at half time step. Whereas the velocity at half time step is calculated from the information of an acceleration at full time step.

$$\mathbf{v}\left(t + \frac{\Delta t}{2}\right) = \mathbf{v}\left(t - \frac{\Delta t}{2}\right) + \mathbf{a}\left(t\right)\Delta t, \tag{3.23}$$

$$\boldsymbol{r}\left(t + \Delta t\right) = \boldsymbol{r}\left(t\right) + \mathbf{v}\left(t + \frac{\Delta t}{2}\right)\Delta t. \tag{3.24}$$

By using (3.23) and (3.24), we obtain a new particle postition in a new time step. For the first time step, the information of velocity at $-\Delta t/2$ can be obtained from Euler backward method

$$\mathbf{v}\left(-\Delta t/2\right) = \mathbf{v}_0 - \frac{1}{2}\mathbf{a}_0\,\Delta t,$$

where $\mathbf{v}_0 = \mathbf{v}(0)$ and $\mathbf{a}_0 = \mathbf{a}(0)$.

The time step (Δt) might be chosen carefully. In order to obtain the stable solution, the time step should satisfy the Courant-Friedrichs-Levy stability condition [16]. The condition due to the speed of sound, c,

$$\Delta t \leq 0.25\,\frac{h}{c},$$

due to the magnitude of individual particle acceleration $\mathbf{a}_i\left(= \frac{D\mathbf{v}_i}{Dt}\right)$,

$$\Delta t \leq 0.25\,\min\left(\frac{h}{|\mathbf{a}_i|}\right)^{\frac{1}{2}}.$$

3.5 Summary

We summarize our procedure for solving the governing equations in SPH method in the following diagram
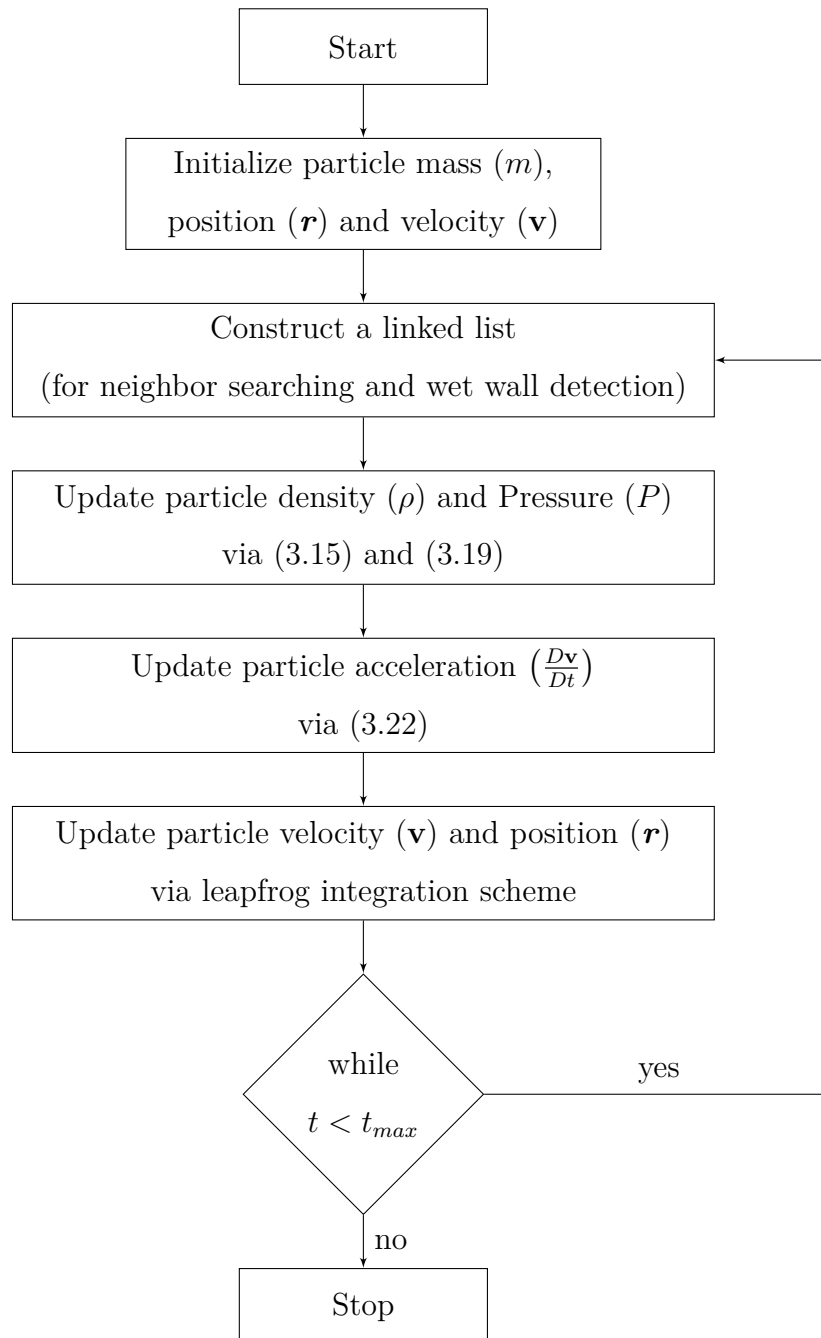
```
                    ┌─────────────────┐
                    │      Start       │
                    └─────────────────┘
                             │
                             ▼
              ┌──────────────────────────────┐
              │ Initialize particle mass (m), │
              │ position (r) and velocity (v) │
              └──────────────────────────────┘
                             │
                             ▼
         ┌────────────────────────────────────────────┐
         │        Construct a linked list              │◄──────┐
         │ (for neighbor searching and wet wall detection)│     │
         └────────────────────────────────────────────┘       │
                             │                                 │
                             ▼                                 │
         ┌────────────────────────────────────────────┐       │
         │ Update particle density (ρ) and Pressure (P)│       │
         │           via (3.15) and (3.19)             │       │
         └────────────────────────────────────────────┘       │
                             │                                 │
                             ▼                                 │
         ┌────────────────────────────────────────────┐       │
         │ Update particle acceleration (Dv/Dt)        │       │
         │              via (3.22)                     │       │
         └────────────────────────────────────────────┘       │
                             │                                 │
                             ▼                                 │
         ┌────────────────────────────────────────────┐       │
         │ Update particle velocity (v) and position (r)│      │
         │       via leapfrog integration scheme        │      │
         └────────────────────────────────────────────┘       │
                             │                                 │
                             ▼                                 │
                        ╱─────────╲       yes                  │
                      ╱   while     ╲─────────────────────────┘
                      ╲  t < t_max  ╱
                        ╲─────────╱
                             │ no
                             ▼
                    ┌─────────────────┐
                    │      Stop        │
                    └─────────────────┘
```

Figure 3.7: Diagram of procedure for solving governing equations

CHAPTER IV

RESULTS AND DISCUSSIONS

In this chapter, the implementation of SPH method combined with surface tension is applied to solve the system equations we have discussed in Chapter 2 and Chapter 3. The 2- and 3-dimensional numerical results of 10, 15, 20, 25, and 30 mg droplets will be shown and compared with experimental results from [20] to verify that our model can describe the phenomenon well.

4.1 2-dimensional Simulation

We start with 2-dimensional system. The parameter used in 2-dimensional simulation are shown in Table 4.1. The 10, 15, 20, 25 and 30 mg droplets are initialized by 440, 576, 729, 840 and 930 particles, respectively in rectangular shape under gravitational force and surface tension force with boundary particles as a wall in order to validate the model via droplet status including retent or moving on vertical plane. The drops fall down a bit for early time step because they have not formed to be regular shape yet, After that, the drops which have a big mass, including 25 and 30 mg droplets continue falling down but 10, 15 and 20 mg droplets stop moving and are hanged on the wall which gives a good agreement with the experimental results. Moreover, the receding angles and advancing angles are measured via Adobe Photoshop CS2 software and compared with experimental results. Here are our model results at $t = 0.5\,s$ validated with experimental results.
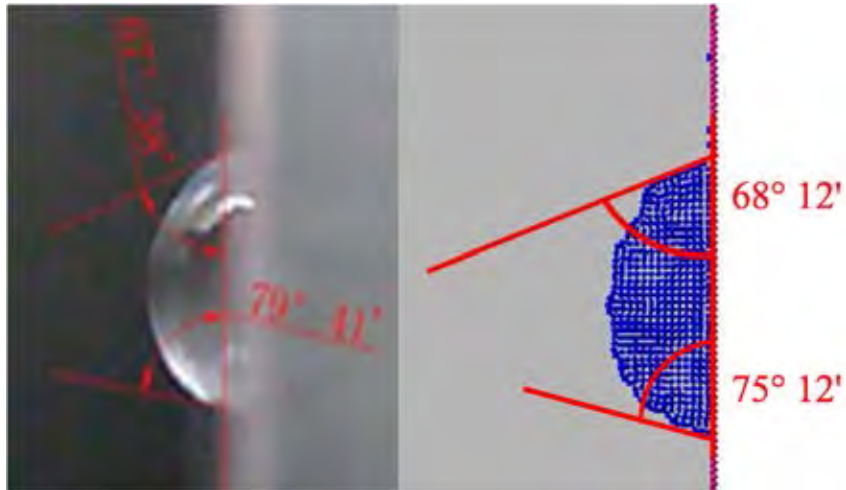
Figure 4.1: The experimental result (left) [20] and 2-dimensional numerical result (right) of 10 mg droplet
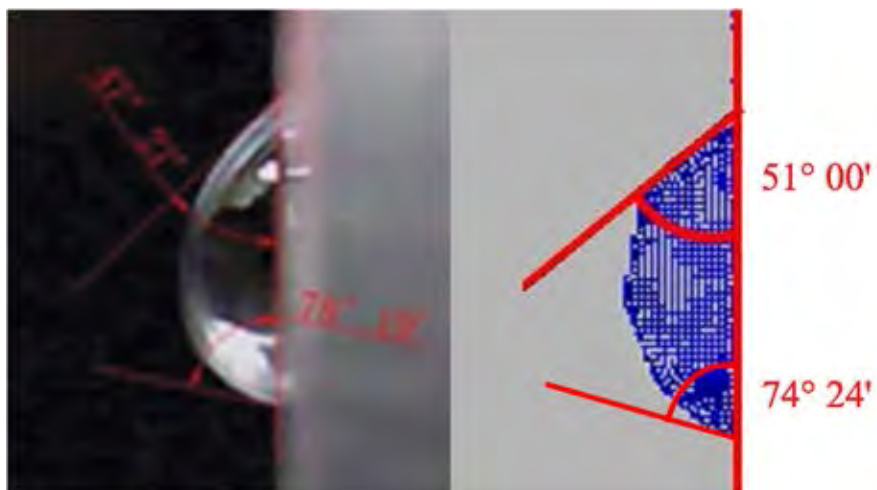

Figure 4.2: The experimental result (left) [20] and 2-dimensional numerical result (right) of 15 mg droplet
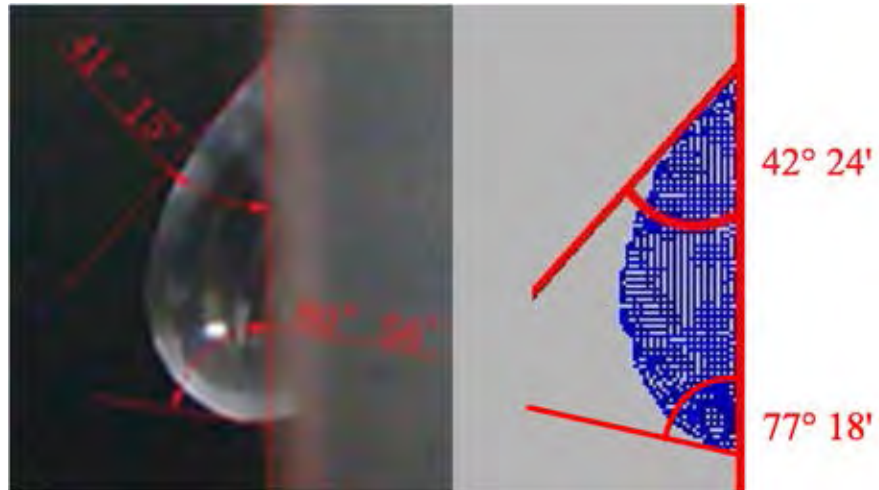
Figure 4.3: The experimental result (left) [20] and 2-dimensional numerical result (right) of 20 mg droplet
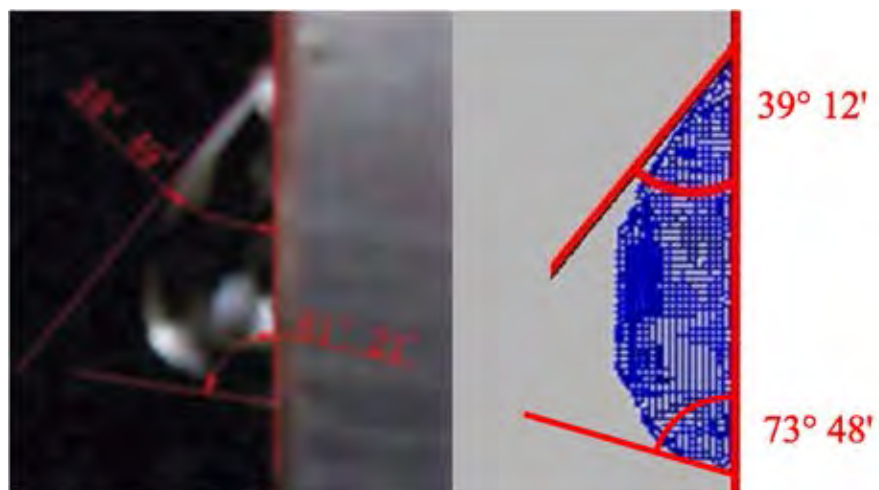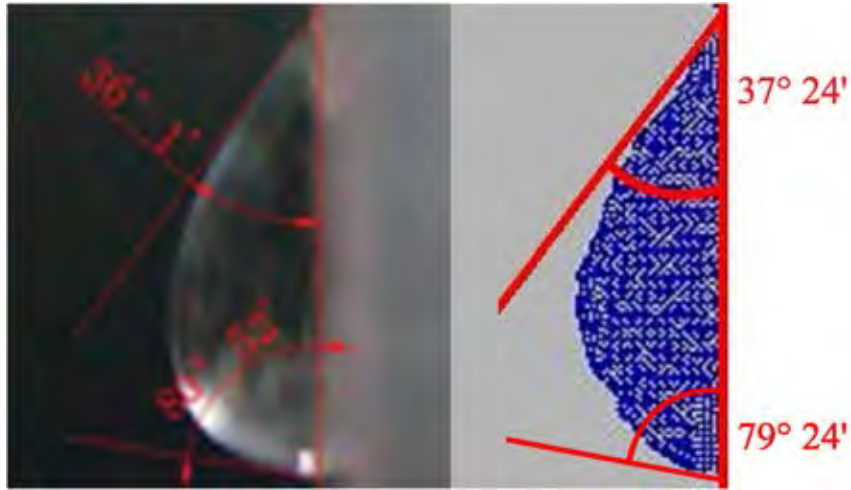

Figure 4.4: The experimental result (left) [20] and 2-dimensional numerical result (right) of 25 mg droplet

Figure 4.5: The experimental result (left) [20] and 2-dimensional numerical result (right) of 30 mg droplet

Table 4.1: The parameters for 2-dimensional simulation

Parameter	Value
Particle mass (m)	9.75693×10^{-6} kg
Reference density (ρ_0)	1000 kg/m^3
Acceleration of gravity (g)	9.8 m/s^2
Speed of sound (c)	15 m/s
Smoothing length (h)	0.0002 m
Time step (Δt)	0.000001 s
s_{ij} for fluid-fluid interaction	0.43
s_{ij} for fluid-wetted solid interaction	0.47
s_{ij} for fluid-not wetted solid interaction	0.32

Table 4.2: The status of droplet compared between experimental results and 2-dimensional numerical results

Mass (mg)	Status	
	Experimental	Numerical
10	Retent	Retent
15	Retent	Retent
20	Retent	Retent
25	Moving	Moving
30	Moving	Moving

From Table 4.2, we can illustrate that the numerical results give the good agreement with the experimental results. The 10, 15, and 20 mg droplets are hanged on the wall because the adhesion, fluid-solid attractive force beats the gravitational force. However, as the droplet mass increases to 25 and 30 mg, the gravitational force acting on the droplet increase as well, providing the adhesion force cannot support the droplet anymore. Thus, the droplet falls down by influence of gravitational force.

From Table 4.3-4.4 and Figure 4.1-4.7, we can infer that the average deviation of receding angles between numerical results and experimental results is 3.15% and the average deviation of advancing angles between numerical results and experimental results is 5.45%. This shows that our model can describe the phenomenon. The maximum deviation of receding angle is 7.48% from 15 mg droplet, it might be caused from we let the droplet falling down before the droplet keeps the shape. This drawback will be fixed in 3-dimensional simulation.

Table 4.3: The receding angles compared between experimental results and 2-dimensional numerical results

	Receding angle		Relative
Mass (mg)	Experimental	Numerical	deviation, %
10	68°38′	68°12′	0.63
15	47°27′	51°00′	7.48
20	41°15′	42°24′	2.78
25	38°49′	39°12′	1.01
30	36°10′	37°24′	3.86
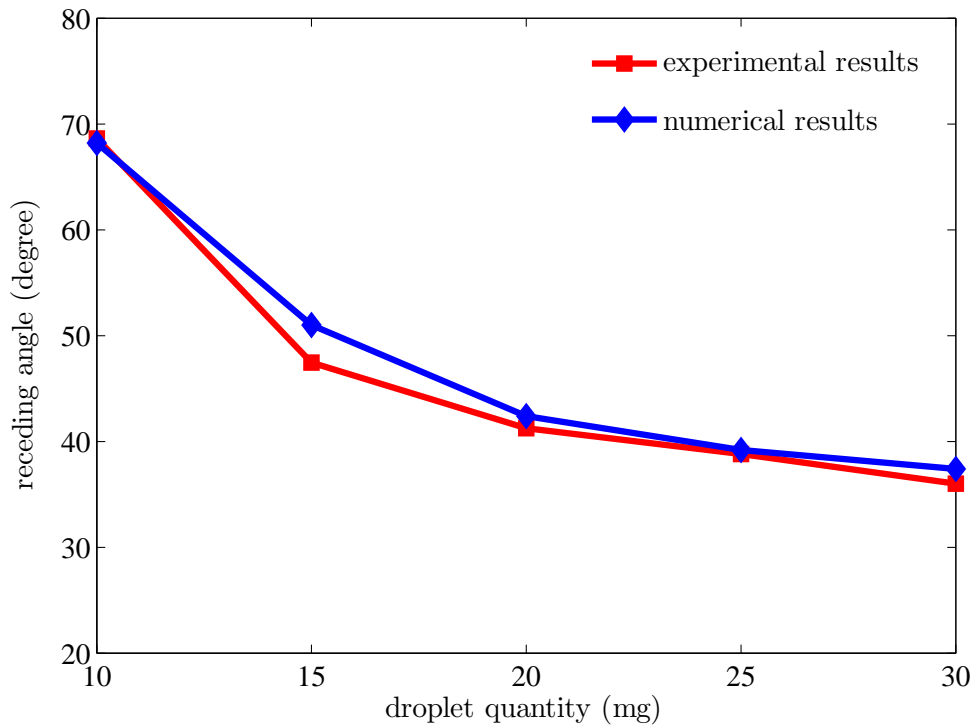
Figure 4.6: The comparison of receding angles between experimental results and 2-dimensional numerical results

Table 4.4: The advancing angles compared between experimental results and 2-dimensional numerical results

| | Advancing angle | | Relative |
Mass (mg)	Experimental	Numerical	deviation, %
10	79°41′	75°12′	5.72
15	78°19′	74°24′	5.21
20	80°56′	77°18′	4.63
25	81°21′	73°48′	9.67
30	80°52′	79°24′	2.02
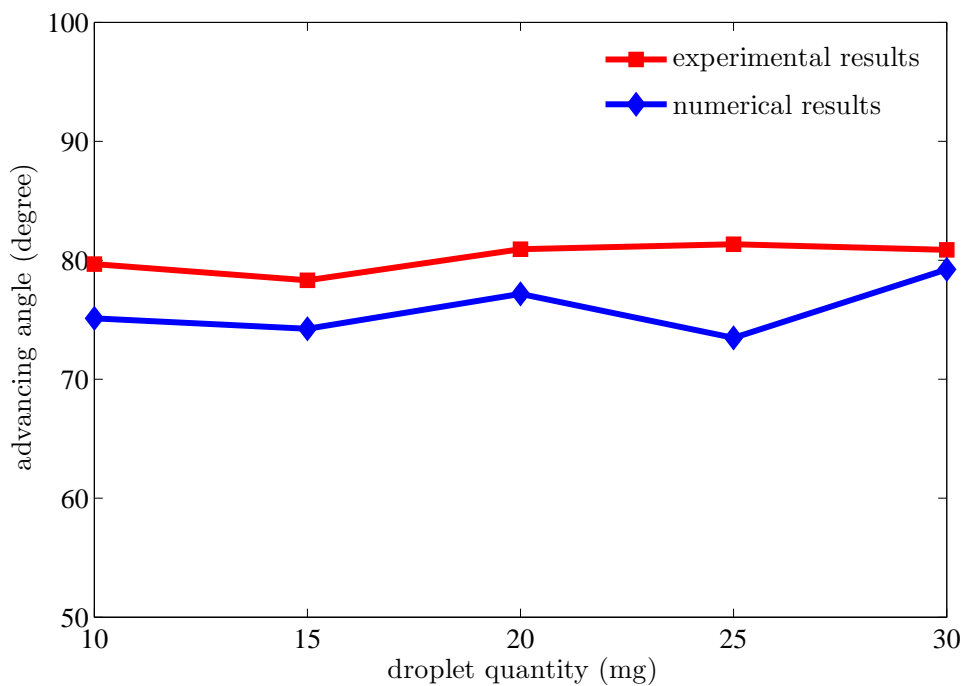
Figure 4.7: The comparison of advancing angles between experimental results and 2-dimensional numerical results

However, the big drawback is the 2-dimensional simulation does not present the realistic droplet mass and volume because it presents only the cross-section of the droplet not the whole droplet. The number of particles we used in 2-dimensional simulation is just represented for the area of cross-section. Hence, we advance our simulation to 3-dimensional system to get more realistic model.

4.2 3-dimensional Simulation

The 3-dimensional simulation is proposed here to improve the model realistically. In the following simulation, the number of particles used to simulate the 10, 15, 20, 25 and 30 mg droplets is 1320, 2016, 2730, 3360 and 4032 particles, respectively in rectangular shape with boundary particles as a wall and the parameters are given in Table 4.5. For 3-dimensional simulation, we do not put the acceleration of gravity, g, on the early time step ($t = 0\text{-}0.05\,s$) for letting the surface tension makes the droplet being the spherical shape. After that, the acceleration of gravity will be added into the domain. The statuses of the droplet are compared with the experimental result. The receding and advancing angles are compared with experimental results as well. Heres are the 3-dimensional results at $t = 0.15\,s$.
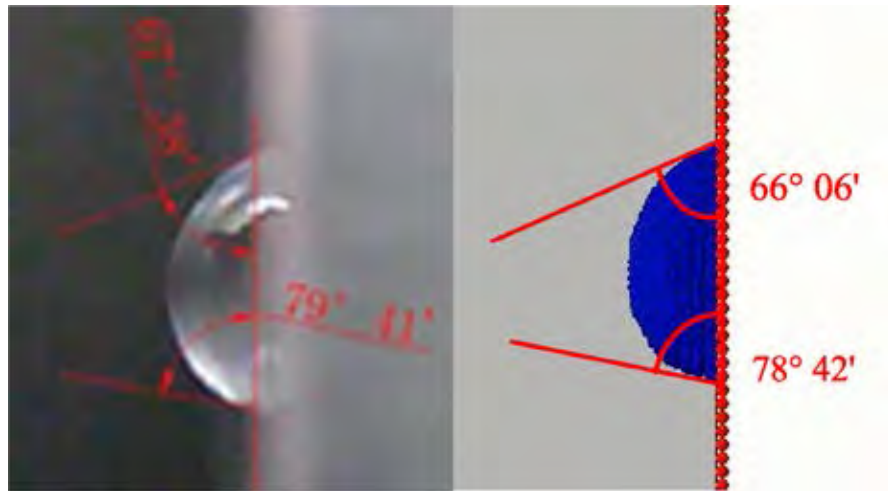
Figure 4.8: The experimental result (left) [20] and 3-dimensional numerical result (side view) (right) of 10 mg droplet
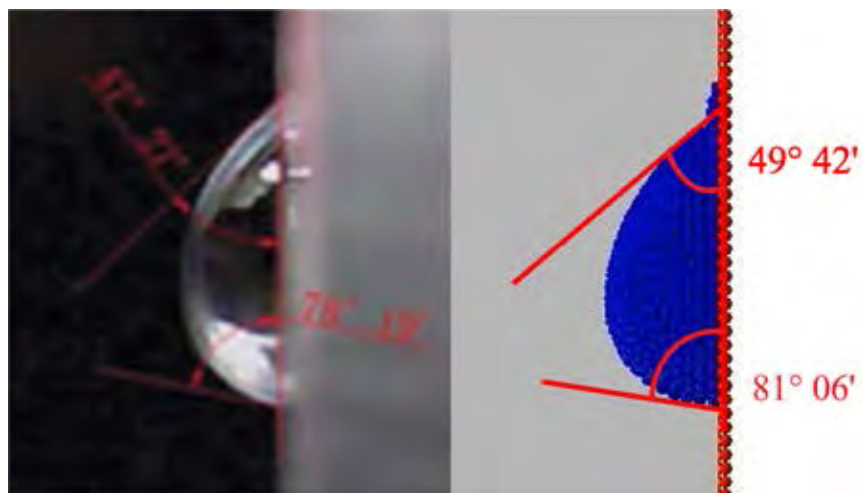

Figure 4.9: The experimental result (left) [20] and 3-dimensional numerical result (side view) (right) of 15 mg droplet
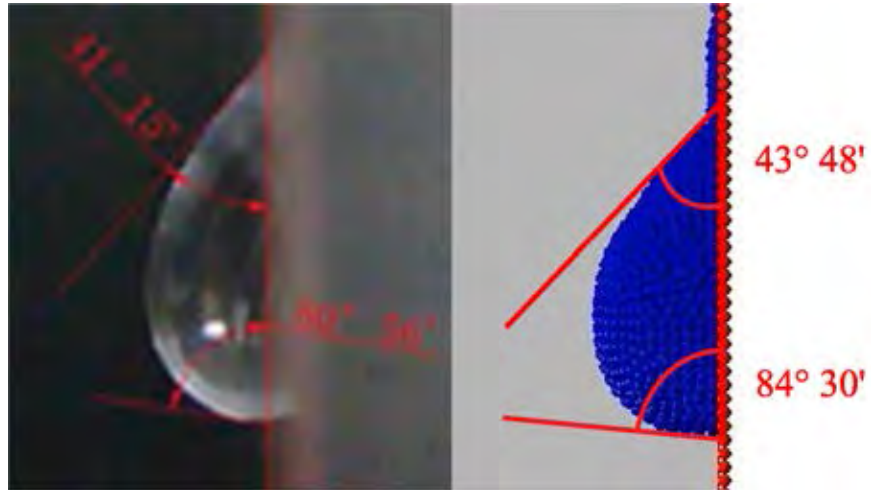
Figure 4.10: The experimental result (left) [20] and 3-dimensional numerical result (side view) (right) of 20 mg droplet
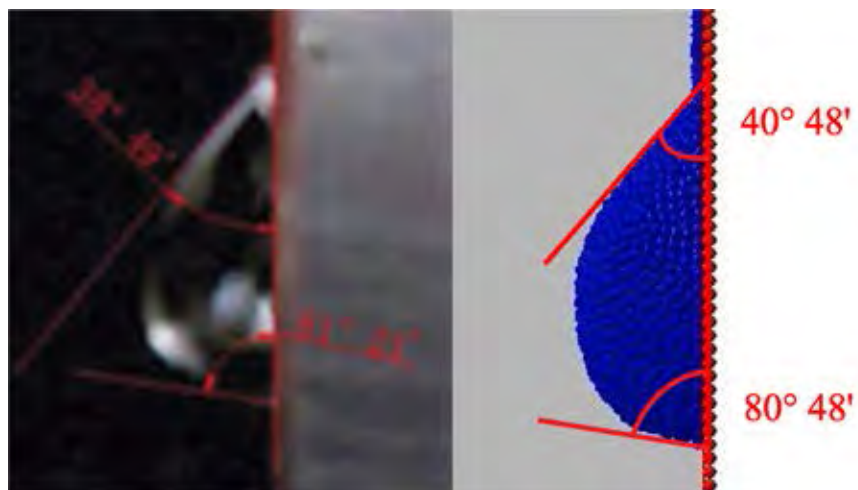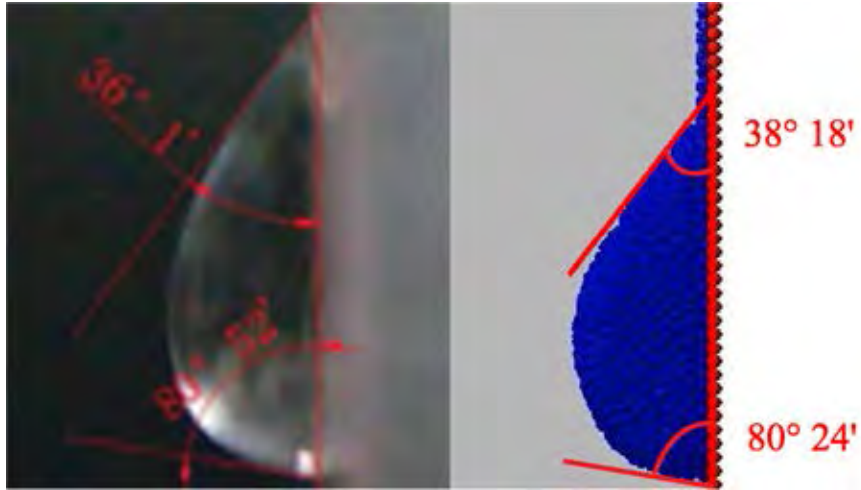

Figure 4.11: The experimental result (left) [20] and 3-dimensional numerical result (side view) (right) of 25 mg droplet

Figure 4.12: The experimental result (left) [20] and 3-dimensional numerical result (side view) (right) of 30 mg droplet

Table 4.5: The parameters for 3-dimensional simulation

Parameter	Value
Particle mass (m)	7.65031×10^{-9} kg
Reference density (ρ_0)	1000 kg/m^3
Acceleration of gravity (g)	9.8 m/s^2
Speed of sound (c)	8 m/s
Smoothing length (h)	0.0004 m
Time step (Δt)	0.00001 s
s_{ij} for fluid-fluid interaction	0.0375
s_{ij} for fluid-wetted solid interaction	0.0375
s_{ij} for fluid-not wetted solid interaction	0.00005

Table 4.6: The status of droplet compared between experimental results and 3-dimensional numerical results

Mass (mg)	Status	
	Experimental	Numerical
10	Retent	Retent
15	Retent	Retent
20	Retent	Retent
25	Moving	Moving
30	Moving	Moving

From Table 4.6, we see the numerical results also give a good agreement with the experimental results on the status of droplet same as 2-dimensional simulation. From 4.7-4.8 and Figure 4.8-4.14, we can illustrate that the average deviation of receding angles between numerical results and experimental results is 5.11% and the average deviation of advancing angles between numerical results and experimental results is 2.16%. This means that our model in 3-dimensional system can also depict the droplet motion on vertical plane. Moreover, we see that there is no big jump error as it has happened in 2-dimensional simulation of 15 mg droplet that its deviation is 7.48%, while the average deviation of receding angles of other simulations is only 2.07%. The 3-dimensional simulation's average deviation of advancing angles is less than the 2-dimensional simulation's. This shows that the 3-dimensional simulation gives better results. Although the 3-dimensional simulation's average deviation of receding angles is more than 2-dimensional simulation's average deviation, it can be seen that it looks more "uniform".

Table 4.7: The receding angles compared between experimental results and 3-dimensional numerical results

| | Receding angle | | Relative |
Mass (mg)	Experimental	Numerical	deviation, %
10	68°38′	66°06′	3.69
15	47°27′	49°42′	4.74
20	41°15′	43°48′	6.18
25	38°49′	40°48′	4.61
30	36°10′	38°18′	6.34
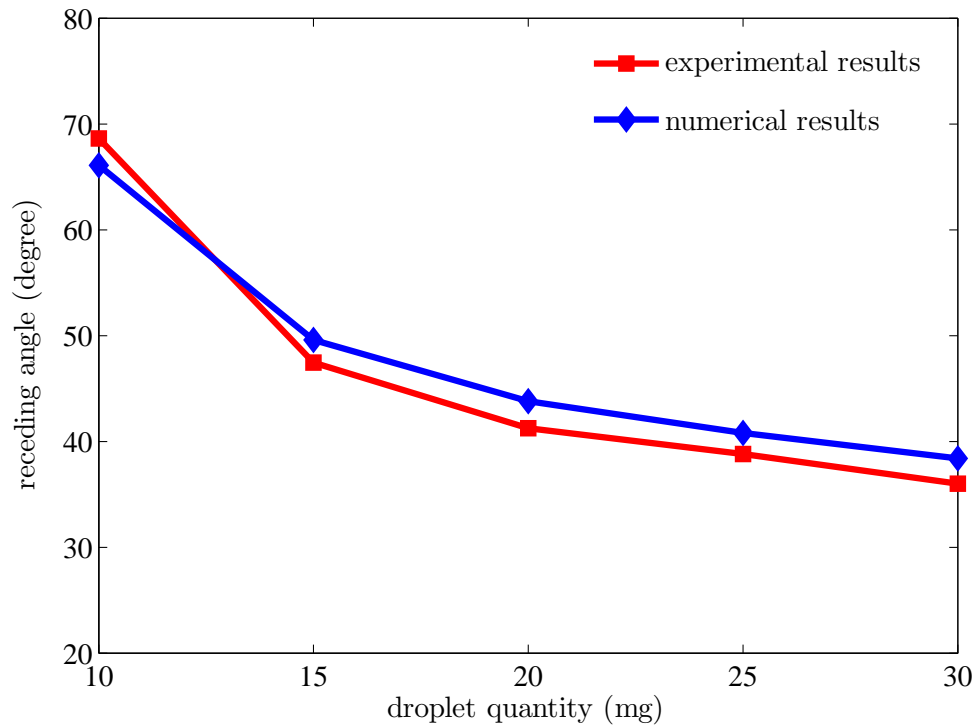
Figure 4.13: The comparison of receding angles between experimental results and 3-dimensional numerical results

Table 4.8: The advancing angles compared between experimental results and 3-dimensional numerical results

Mass (mg)	Advancing angle		Relative deviation, %
	Experimental	Numerical	
10	79°41′	78°42′	1.36
15	78°19′	81°06′	3.55
20	80°56′	43°30′	4.41
25	81°21′	80°48′	0.92
30	80°52′	80°24′	0.58
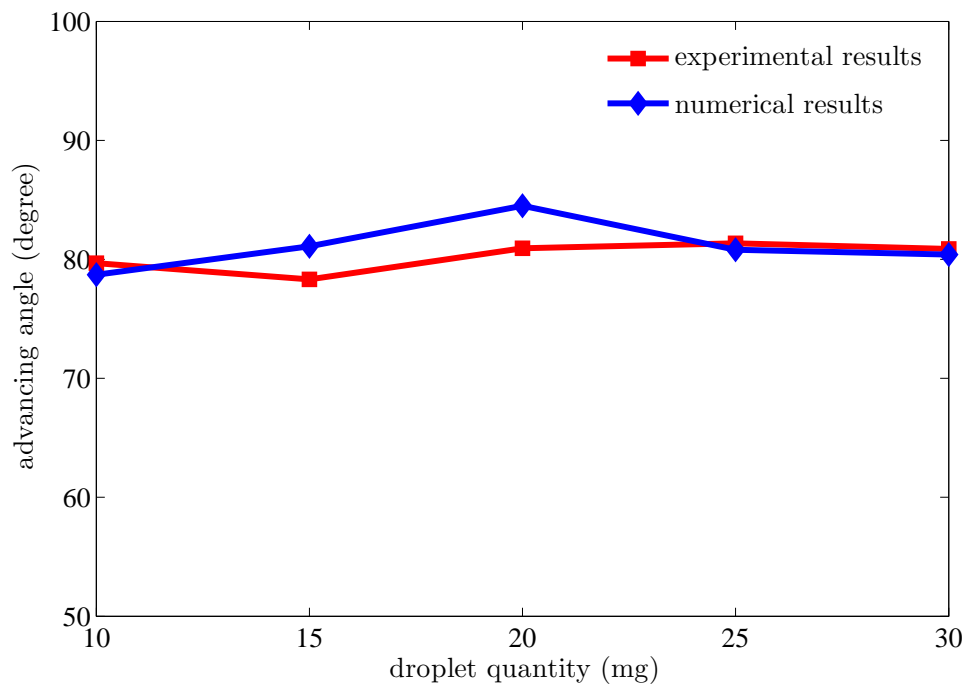
Figure 4.14: The comparison of advancing angles between experimental results and 3-dimensional numerical results

The drawback from 2-dimensional simulation that it cannot catch up the real mass is fixed here. It can be seen that the 10 mg droplet is simulated by 1320 particles with 7.65031×10^{-9} kg/particle. Hence, the simulated mass $\approx$ 10.098 mg. That provides close to real mass whereas the numerical results still can depict the droplet behavior well. Therefore, we can say that our 3-dimensional simulation can describe the real world phenomenon with real scale model.

The receding angles at each time step are measured here to observe the behavior of the droplet. Starting from the time step $t = 0.05\,s$, which is the time step we put the acceleration of gravity, g, into the domain, to $t = 0.15\,s$, which is the end of our simulation. The results show that the receding angles of the 10 and 15 mg droplets decrease slightly from the starting time step. For the 20, 25, and 30 mg droplets, the receding angles decrease dramatically in the early step, then change slightly because the droplets were falling down (the 20 mg droplet fell down a bit and stop) from the effect of gravity. The results are shown in Figure 4.15 - 4.19.
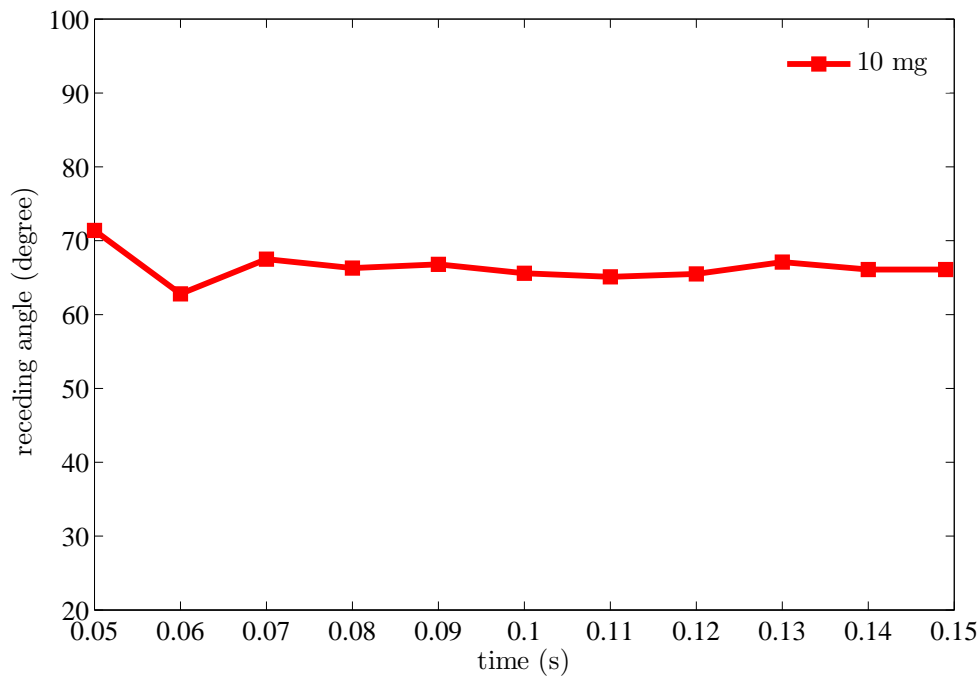

Figure 4.15: The receding angles at each time step of 10 mg droplet
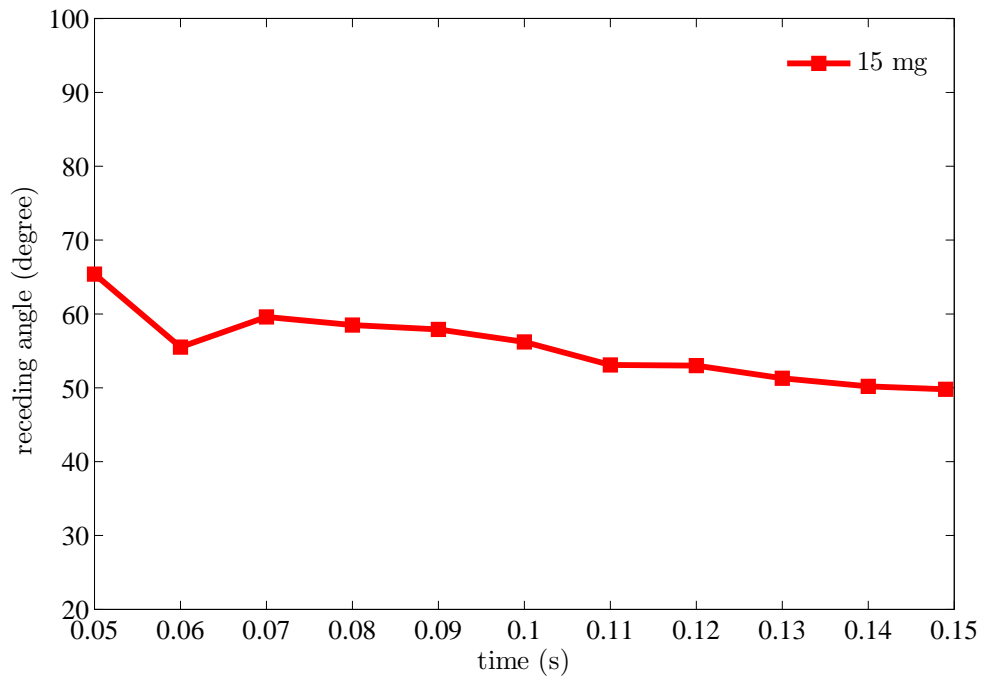
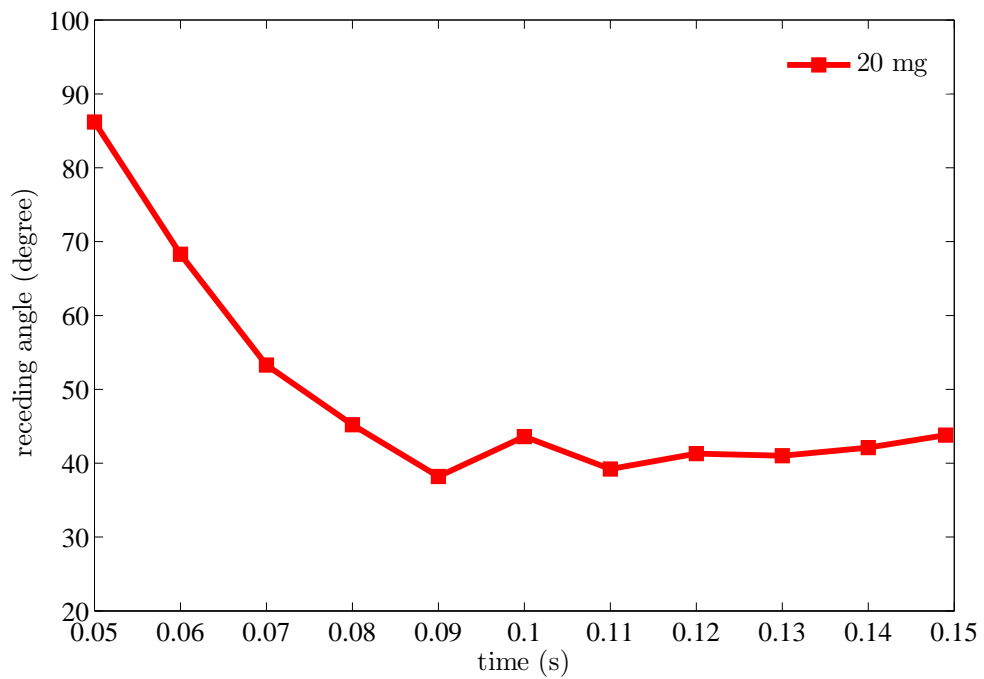Figure 4.16: The receding angles at each time step of 15 mg droplet

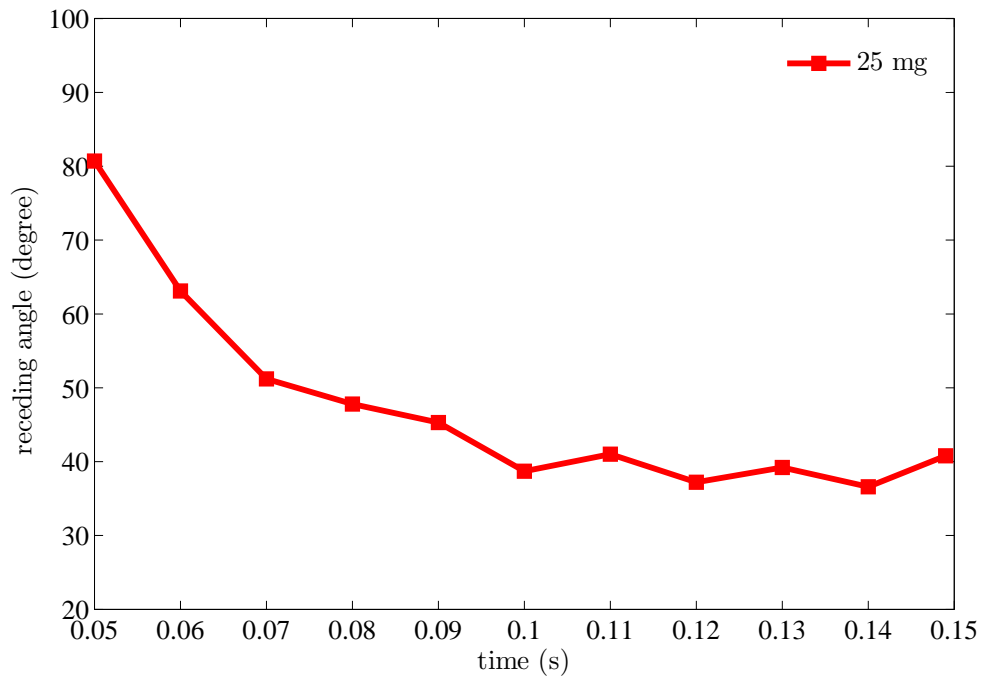Figure 4.17: The receding angles at each time step of 20 mg droplet

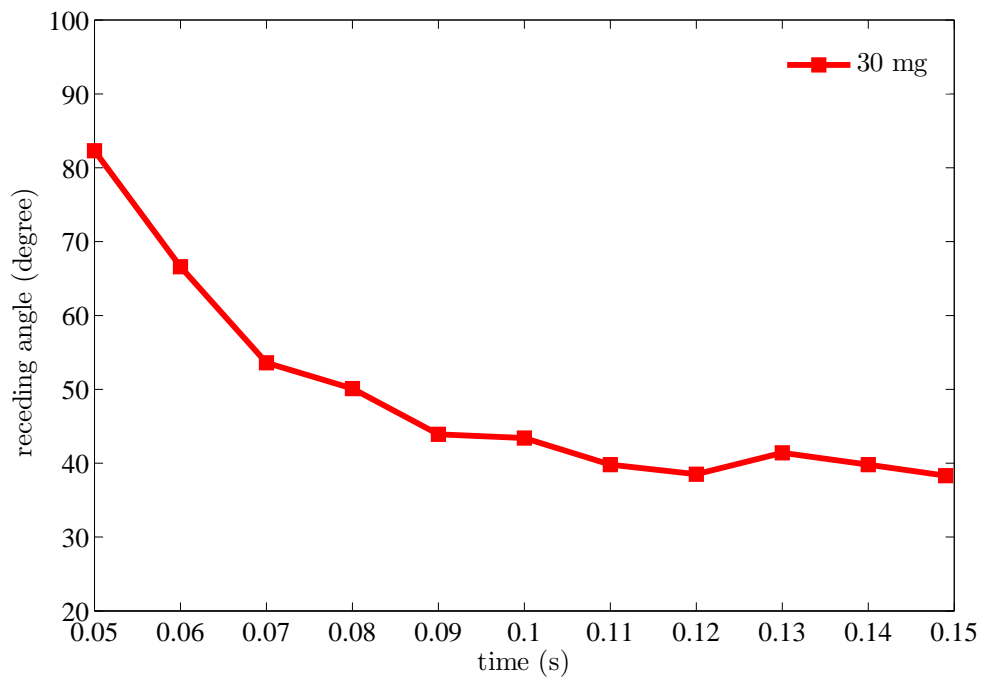Figure 4.18: The receding angles at each time step of 25 mg droplet

Figure 4.19: The receding angles at each time step of 30 mg droplet

The 12.5, 17.5, 22.5, and 27.5 mg droplets are simulated. The receding and advancing angles are measured and appended to the Figure 4.13 and 4.14 to see more apparent how the curve from the numerical results fit the curve from the experimental results. The results are shown in Table 4.9 and Figure 4.20-4.25

Table 4.9: The receding and advancing angles of 3-dimensional numerical results

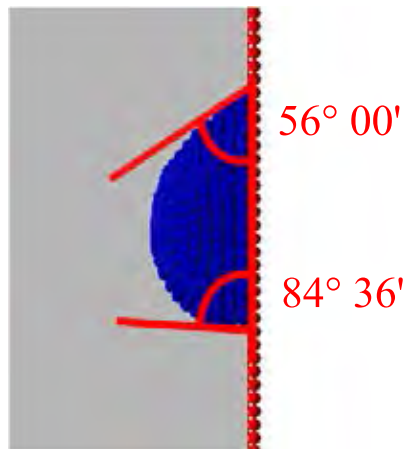| Mass (mg)	Receding angle	Advancing angle
12.5	56°00′	84°36′
17.5	47°36′	85°18′
22.5	42°48′	78°18′
27.5	39°00′	79°36′

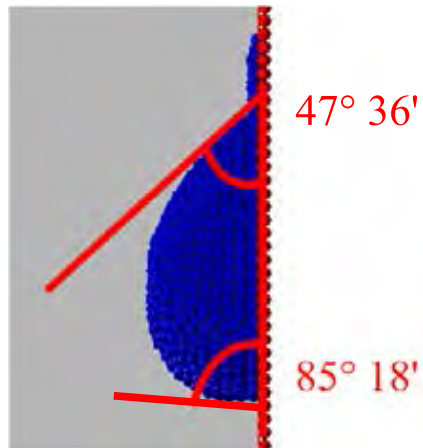Figure 4.20: The 3-dimensional simulation of 12.5 mg droplet

Figure 4.21: The 3-dimensional simulation of 17.5 mg droplet
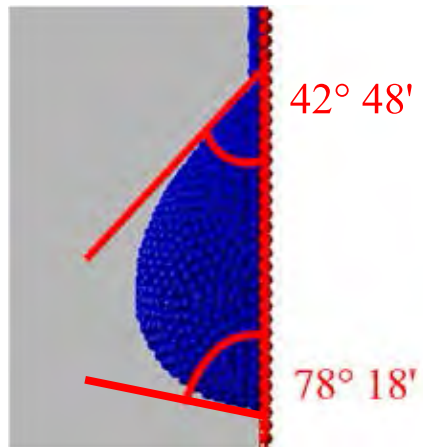

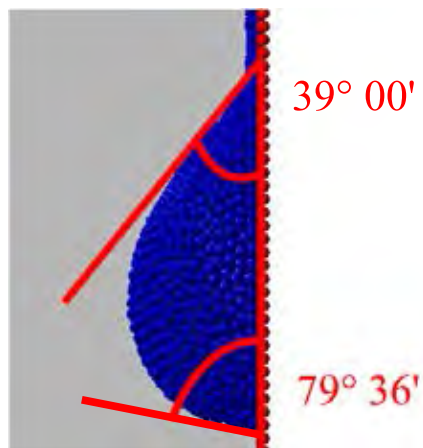Figure 4.22: The 3-dimensional simulation of 22.5 mg droplet

Figure 4.23: The 3-dimensional simulation of 27.5 mg droplet

Figure 4.24: The comparison of receding angles between experimental results and 3-dimensional numerical results with 12.5, 17.5, 22.5, and 27.5 mg appended

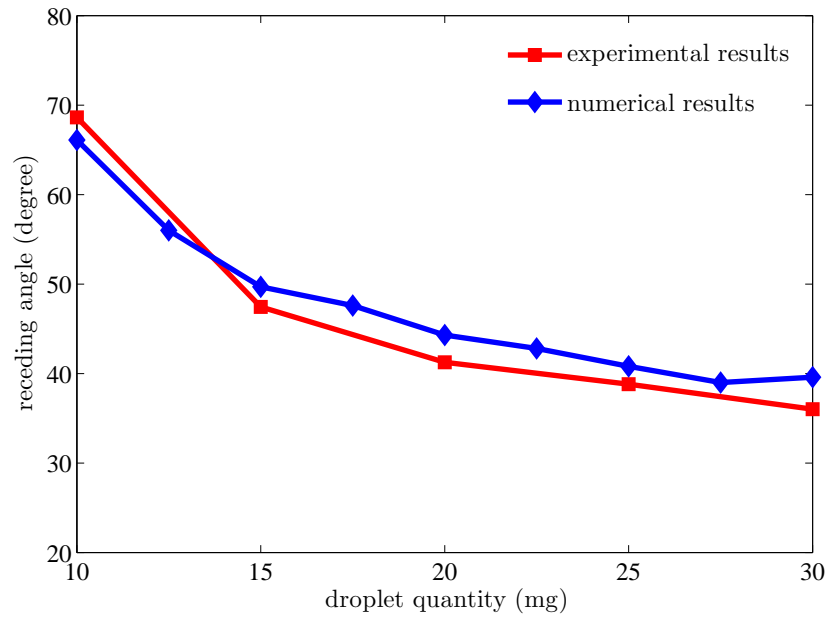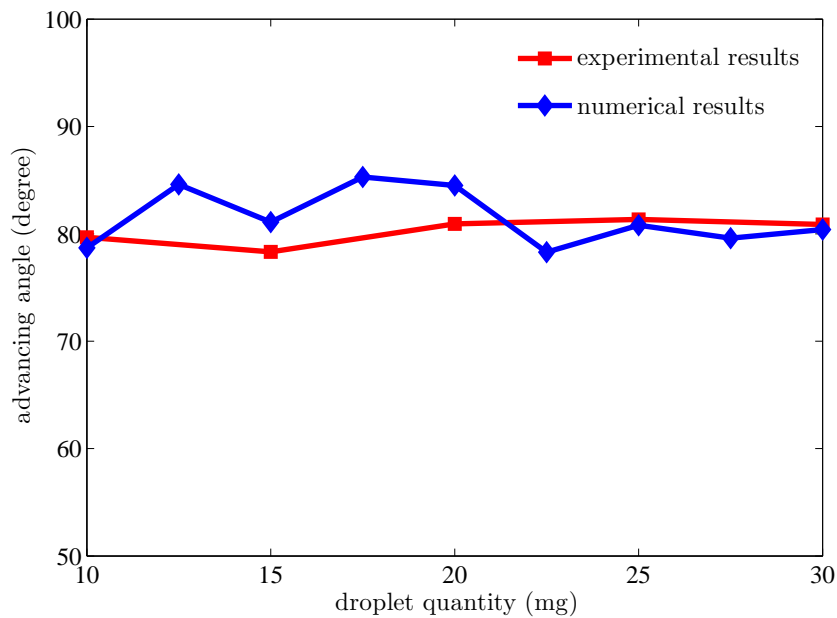
Figure 4.25: The comparison of advancing angles between experimental results and 3-dimensional numerical results with 12.5, 17.5, 22.5, and 27.5 mg appended

CHAPTER V

CONCLUSIONS

5.1 Conclusions of This Work

In this work, the 2- and 3-dimensional simulation of droplet motion on vertical plane using Smoothed Particle Hydrodynamics (SPH) method combined with surface tension has been introduced. The surface tension which modeled from a particle-particle interaction can be integrated into standard SPH method.

We can conclude that SPH is a powerful tool used in fluid simulation as the following benefits. Since we discretized the fluid into particles, SPH guarantees conservation of mass automatically (if the particles do not fly away from our domain). The free surface is easy to track because the particles directly create the fluid phase while the empty space stands for the air phase. Another benefit is easy to implement, that is, we need not be related with mesh formulation, which is practically difficult part in grid-based method at all.

From the numerical results we have presented in the previous chapter, we can see that our simulations in both 2 and 3 dimensions successfully describe the droplet profile and behavior. The receding and advancing angles of the 10, 15, 20, 25, and 30 mg droplets are measured and compared with the experiment from [20]. The model validations show that the receding and advancing angles obtained from SPH simulation give a good agreement with those obtained from experiment. The average deviations of receding angles are 3.15% and 5.11% for 2- and 3- dimensional simulations, respectively, and the average deviation of advancing angles are 5.45% and 2.07% for 2- and 3- dimensional simulations, respectively. The status of droplet is verified as well. In our simulations, for 10, 15, and 20 mg droplets, their status are retent which are the same as the experiment and for 25 and 30 mg droplets their status are moving which are also the same as the experiment.

The overall angle of the droplet at each time step are shown to observe how the droplet's angle change in time. For the droplet that is retent, the angle decreases slightly but for the droplet that is moving, the angle decrease dramatically in early step. The 12.5, 17.5, 22.5, and 27.5 mg droplets which are between 10, 15, 20, 25, and 30 mg, are simulated to see the correspondence with the curve of receding and advancing angles obtained from experiment. They give a good agreement as well.

The disadvantage of 2-dimensional simulation is that it cannot give the real droplet mass and volume. It only presented the area of droplet cross-section area. For more realistic model, the 3-dimensional simulation can suppress this disadvantage. The number of particles and particle mass used in 3-dimensional simulation correspond to the real droplet mass as we have shown in the case of 10 mg droplet. Therefore, we can conclude that our simulation can model the problem in real world scale.

5.2 Future Works

In this section, we propose the plan for the future works to improve the results or extend the scope of the research. We list the plans as follows

1. To boost up the overall computing performance, the graphics processing unit (GPU) will be used. It has been deployed widely over a last decade for dramatic increasing the computing performance.

2. The neighbor particle searching in every time step costed a great computational time. It can be reduced if we can improve how to handle the neighbor searching.

3. The wet detection which deals with the wall particles is not quite good. The algorithm we used is presuming all particles in a cell that is contiguous with fluid particle are wet. We need more specific method to improve the wet detection algorithm. More accurate detecting the wet particle, more accurate modeling the surface tension.

4. Although the surface tension model that we have employed gave good results, anyway, there are many techniques used to model the surface tension. Trying another model may give a better result.

REFERENCES

[1] Batchelor, G. K. (1967): *An Introduction to Fluid Dynamics*, Cambridge University Press, Cambridge.

[2] Brackbill, J. U., Kothe, D. B., and Zemach, C. (1994): Continuum Method for Modelling Surface Tension, *Journal of Computational Physics* 100: 335–354.

[3] Capone, T.: *SPH Numerical Modelling of Impulse Water Waves Generated by Landslides* [Online]. 2009. Available from: http://cfd.mace.manchester.ac.uk/sph/SPH_PhDs/2009/CaponeThesis.pdf [2014, October].

[4] Das, A. K., and Das, P. K. (2009): Simulation of Drop Movement over an Inclined Surface using Smoothed Particle Hydrodynamics, *Langmuir* 25: 11459–66.

[5] Jafary, M., and Khandekar, S.: *Simulation of Droplets on Inclined Surfaces using Smoothed Particle Hydrodynamics* [PDF]. 2011. Available from: http://home.iitk.ac.in/~samkhan/Bio_data/publications/Khandekar_Conf_31.pdf [2014, October].

[6] Bush, J. W. M.: *MIT Lecture Notes on Surface Tension, lecture 1* [PDF]. 2007. Available from: http://web.mit.edu/1.63/www/Lec-notes/Surfacetension/Lecture1.pdf[2014, November].

[7] Kelager, M.: *Lagrangian Fluid Dynamics Using Smoothed Particle Hydrodynamics* [PDF]. 2006. Available from: http://image.diku.dk/projects/media/kelager.06.pdf [2014, October].

[8] Liu, G. R., and Liu, M. B. (2003): *Smoothed Particle Hydrodynamics: A Meshfree Particle Method*, World Scientic Publishing Co. Pte. Ltd., Singapore.

[9] Lucy, L. B. (1977): A Numerical Approach to the Testing of the Fission Hypothesis , *Journal of Astronomy* 82(12): 1013–1024.

[10] Merte, H. Jr., and Yamali, C. (1983): Profile and Departure Size of Condensation Drops on Vertical Surface, *Wärme-Stoffübertrag* 17: 171–180.

[11] Milinazzo, F., and Shinbrot, M. (1988): A Numerical Study of a Drop on a Vertical Wall , *Journal Colloid Interface* 25: 254–264.

[12] Monaghan, J. J. (1988): An Introduction to SPH. *Computer Physics Communication* 48: 88–96.

[13] Monaghan, J. J. (1992): Smoothed Particle Hydrodynamics. *Annual Review of Astronomical and Astrophysics* 30: 543–574.

[14] Monaghan, J. J. (2005): Smoothed Particle Hydrodynamics. *Rep. Prog. Phys.* 68: 1703–1759.

[15] Morris, J. P., Fox, P. J., and Zhu, Y. (1997): Modeling Low Reynolds Number Incompressible Flows using SPH. *Journal of Computational Physics* 136: 214–226.

[16] Morris, J. P. (2000): Simulating Surface Tension with Smoothed Particle Hydrodynamics. International *Journal for Numerical Methods in Fluid* 33: 333–353.

[17] Nugent, S., and Posch, H. A. (2000): Liquid Drops and Surface Tension with Smoothed Particle Applied Mechanics. *Physical Review* 62(4): 4968–4975.

[18] Nvineeth: *Photo of Hibiscus rosa-sinensis, Camera: canon powershot a95.* [Self-photographed]. 2006. Available from: http://commons.wikimedia.org/wiki/File:Hibiscus_pink.jpg [2014, November].

[19] Tartakovsky, A., and Meakin, P. (2005): Modeling of Surface Tension and Contact Angles with Smoothed Particle Hydrodynamics. *Physical Review* 72(2): 1–5.

[20] Zhuang, D., Hu, H., Ding G., Xi, G., and Han, W. (2014): Numerical model for liquid droplet motion on vertical plain-fin surface. *HVAC&R Research* 20(3): 332–343.

VITA

Name   Mr. Chaiyod Kamthorncharoen

Date of Birth   19 May 1990

Place of Birth   Bangkok, Thailand

Education   B.Sc. (Mathematics)(First Class Honours),
                     Kasetsart university, 2011

Scholarship   Development and Promotion of Science and Technology
                     Talents Project (DPST)